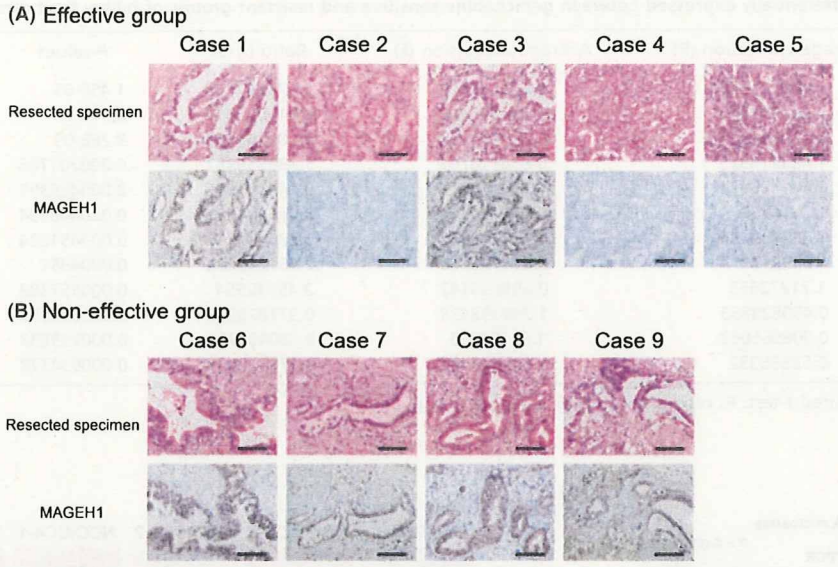


**Fig. 4.** Immunohistochemical analysis of MAGEH1 protein in primary tumor specimens of gemcitabine (Gem)-effective and non-effective groups. Tumor histology (H&E staining) of primary tumor specimens, split into Gem-effective (A) and Gem-non-effective (B) groups and MAGEH1 protein expression detected by anti-MAGEH1 antibody in the same area are shown. All three cases that lacked MAGEH1 expression belong to the Gem-effective group. Scale line = 200 μm.

molecule 6 (CEACAM6) for intrahepatic cholangiocarcinoma,[5] and RRM1 for biliary tract carcinoma.[15] Among these previously reported biomarkers, our microarray analysis validated that RRM2 expression was significantly ($P = 0.03$) increased (three-fold on average) in the resistant group compared to the sensitive one (data not shown). However, most of these studies analyzed a small number of cell lines (maximum two), for example, comparing a gemcitabine-sensitive cancer cell line with its subclone that had acquired gemcitabine resistance, and focused on molecules that are already known to be associated with gemcitabine transport and metabolism. No study has yet tested its efficacy in clinical samples. The present study examined the largest number of BTC cell lines to be detailed in published reports to date, including six novel ones, in relation to clinicopathological information. To discover potential biomarkers in an unbiased way, we examined genome-wide expression profiles using a microarray, identified several biomarker candidates including MAGEH1, and validated its significance in another cohort of clinical BTC cases.

MAGEH1 is a member of the melanoma antigen family (MAGE)[16]. The human MAGE family was originally identified as a tumor-specific antigen,[17] and is now classified into two subtypes (type I and type II).[18] Type I MAGE is completely silenced in normal tissues except male germ cells and placenta, whereas type II MAGE is expressed in both tumors and a fraction of normal tissues. MAGEH1 belongs to the type II MAGE family and is also expressed in normal human tissues.[16] MAGEH1 is expressed in 69% of NSCLC[19] and in 100% of renal cell carcinomas,[20] but no data for BTC have been reported. MAGEH1 associates with the intracellular domain of the p75/NGF receptor[21] and regulates the cell cycle,[19] but its precise role in cancer is largely unknown. In the Gene Expression Omnibus (GEO) database at National Center for Biotechnology Information (NCBI) (http://www.ncbi.nlm.nih.gov/geo/), there is one set of public microarray data showing the association between MAGEH1 expression and gemcitabine resistance in NSCLC cells. Comparison of the gene expression profile of parental Calu3 cell with those of gemcitabine-resistant subclones (Calu3-GemR) revealed that the mean expression of MAGEH1 mRNA in Calu3-GemR clones was more than twice as high as that in the parental cells.[22] However, there was no significant difference between the two, probably because of the small sample size analyzed ($P = 0.2481$; Fig. S1).

We further investigated whether MAGEH1 protein expression can be used for predicting clinical response to gemcitabine treatment, as protein expression is more stable and easier to test in clinical samples than RNA expression. Consistent with the mRNA expression data, we found that MAGEH1 protein was expressed in all resistant and non-effective cases. However, MAGEH1-positive cases also included a portion of sensitive or effective cases, possibly because of post-translational regulation of MAGEH1 protein expression. Significantly, however, MAGEH1-negative cell lines and primary cases were all gemcitabine-sensitive or effective cases, suggesting that MAGEH1 expression could be used as a negative predictor of gemcitabine response. That is, if immunohistochemical staining for MAGEH1 is negative, it is highly likely that a particular case would respond to gemcitabine therapy. Based on its previously reported functions, it remains unclear why MAGEH1 expression would be inversely correlated with gemcitabine response. It could function as a regulator of gemcitabine metabolism or might simply be a surrogate marker of distinct BTC subtypes. Because we analyzed only cases for which the result of gemcitabine treatment had been assessed objectively, it was difficult to collect a large number of retrospective cases. Moreover, we were unable to examine the expression of MAGEH1 RNA in the clinical specimens by RT-PCR because only small amounts of the frozen samples were available. Therefore, further prospective analysis of a larger cohort will be necessary to determine the clinical efficacy of MAGEH1 expression as a predictive biomarker of gemcitabine response.

Recently, a report has indicated that both the amount of stroma and vascularity in the tumor are associated with gemcitabine sensitivity in pancreatic cancer.[23] It was proposed that the hypovascularity and poor vascular architecture of pancreatic ductal carcinomas might impose an additional limitation to therapeutic delivery. Therefore, it was hypothesized that disrupting the stroma of pancreatic tumors might alter the vascular network

and thereby facilitate the delivery of chemotherapeutic agents. Accordingly, we recognized that the tumors in the non-effective group showed a tendency to have more of the stromal component than the tumors in the effective group (Fig. 4). Thus the stromal component would also play an important role in drug resistance of BTC.

In spite of the limited number of cases we examined, our result is consistent with the idea that more complex mechanisms regulate the gemcitabine sensitivity of BTC. In this sense, combination of other biomarker candidates obtained from the present screening or ones discovered through different approaches such as proteomic analysis with MAGEH1 should predict the drug response more accurately. In any event, the present study has shown that our new resource with clinical annotation would be valuable for discovering new biomarkers, and future studies for identifying new therapeutic/diagnostic targets are warranted.

## Acknowledgments

This work was supported by a Grant-in-Aid for Cancer Research from the Ministry of Health, Labor and Welfare of Japan, a Grant-in-Aid for the Third Term Comprehensive 10-Year Strategy for Cancer Control from the Ministry of Health, Labor and Welfare of Japan, and a grant from the program for Promotion of Fundamental Studies in Health Sciences of the National Institute of Biomedical Innovation.

## References

1 Washburn WK, Lewis WD, Jenkins RL. Aggressive surgical resection for cholangiocarcinoma. *Arch Surg* 1995; **130**: 270–6.
2 Kosuge T, Yamamoto J, Shimada K, Yamasaki S, Makuuchi M. Improved surgical results for hilar cholangiocarcinoma with procedures including major hepatic resection. *Ann Surg* 1999; **230**: 663–71.
3 Jang JY, Kim SW, Park DJ *et al.* Actual long-term outcome of extrahepatic bile duct cancer after surgical resection. *Ann Surg* 2005; **241**: 77–84.
4 Sakamoto Y, Kosuge T, Shimada K *et al.* Prognostic factors of surgical resection in middle and distal bile duct cancer: an analysis of 55 patients concerning the significance of ductal and radial margins. *Surgery* 2005; **137**: 396–402.
5 Ieta K, Tanaka F, Utsunomiya T, Kuwano H, Mori M. CEACAM6 gene expression in intrahepatic cholangiocarcinoma. *Br J Cancer* 2006; **95**: 532–40.
6 Khan SA, Thomas HC, Davidson BR, Taylor Robinson SD. Cholangiocarcinoma. *Lancet* 2005; **366**: 1303–14.
7 Thongprasert S. The role of chemotherapy in cholangiocarcinoma. *Ann Oncol* 2005; **16** (Suppl 2): ii93–6.
8 Shi X, Liu S, Kleeff J, Friess H, Buchler MW. Acquired resistance of pancreatic cancer cells towards 5-Fluorouracil and gemcitabine is associated with altered expression of apoptosis-regulating genes. *Oncology* 2002; **62**: 354–62.
9 Eisenhauer EA, Therasse P, Bogaerts J *et al.* New response evaluation criteria in solid tumours: revised RECIST guideline (version 1.1). *Eur J Cancer* 2009; **45**: 228–47.
10 Nakano Y, Tanno S, Koizumi K *et al.* Gemcitabine chemoresistance and molecular markers associated with gemcitabine transport and metabolism in human pancreatic cancer cells. *Br J Cancer* 2007; **96**: 457–63.
11 Duxbury MS, Ito H, Zinner MJ, Ashley SW, Whang EE. RNA interference targeting the M2 subunit of ribonucleotide reductase enhances pancreatic adenocarcinoma chemosensitivity to gemcitabine. *Oncogene* 2004; **23**: 1539–48.
12 Mori Iwamoto S, Kuramitsu Y, Ryozawa S *et al.* Proteomics finding heat shock protein 27 as a biomarker for resistance of pancreatic cancer cells to gemcitabine. *Int J Oncol* 2007; **31**: 1345–50.
13 Rosell R, Danenberg KD, Alberola V *et al.* Ribonucleotide reductase messenger RNA expression and survival in gemcitabine/cisplatin-treated advanced non-small cell lung cancer patients. *Clin Cancer Res* 2004; **10**: 1318–25.
14 Santini D, Perrone G, Vincenzi B *et al.* Human equilibrative nucleoside transporter 1 (hENT1) protein is associated with short survival in resected ampullary cancer. *Ann Oncol* 2008; **19**: 724–8.
15 Ohtaka K, Kohya N, Sato K *et al.* Ribonucleotide reductase subunit M1 is a possible chemoresistance marker to gemcitabine in biliary tract carcinoma. *Oncol Rep* 2008; **20**: 279–86.
16 Chomez P, De Backer O, Bertrand M, De Plaen E, Boon T, Lucas S. An overview of the MAGE gene family with the identification of all human members of the family. *Cancer Res* 2001; **61**: 5544–51.
17 van der Bruggen P, Traversari C, Chomez P *et al.* A gene encoding an antigen recognized by cytolytic T lymphocytes on a human melanoma. *Science* 1991; **254**: 1643–7.
18 Barker PA, Salehi A. The MAGE proteins: emerging roles in cell cycle progression, apoptosis, and neurogenetic disease. *J Neurosci Res* 2002; **67**: 705–12.
19 Tsai JR, Chong IW, Chen YH *et al.* Differential expression profile of MAGE family in non-small-cell lung cancer. *Lung Cancer* 2007; **56**: 185–92.
20 Kramer BF, Schoor O, Kruger T *et al.* MAGED4-expression in renal cell carcinoma and identification of an HLA-A*25-restricted MHC class I ligand from solid tumor tissue. *Cancer Biol Ther* 2005; **4**: 943–8.
21 Tcherpakov M, Bronfman FC, Conticello SG *et al.* The p75 neurotrophin receptor interacts with multiple MAGE proteins. *J Biol Chem* 2002; **277**: 49101–4.
22 Tooker P, Yen WC, Ng SC *et al.* Bexarotene (LGD1069, Targretin), a selective retinoid X receptor agonist, prevents and reverses gemcitabine resistance in NSCLC cells by modulating gene amplification. *Cancer Res* 2007; **67**: 4425–33.
23 Olive KP, Jacobetz MA, Davidson CJ *et al.* Inhibition of Hedgehog signaling enhances delivery of chemotherapy in a mouse model of pancreatic cancer. *Science* 2009; **324**: 1457–61.

## Supporting Information

Additional Supporting Information may be found in the online version of this article:

**Fig. S1.** Mircoarray data of association between MAGEH1 and gemcitabine in non-small lung cancer from NCBI GEO database.

**Table S1.** Primers for mutation analysis of *p53* and *KRAS* genes.

**Table S2.** Clinicopathological feature of 9 patients.

Please note: Wiley-Blackwell are not responsible for the content or functionality of any supporting materials supplied by the authors. Any queries (other than missing material) should be directed to the corresponding author for the article.



doi: 10.1111/j.1349-7006.2009.01462.x

# Intraductal carcinosarcoma with a heterologous mesenchymal component originating in intraductal papillary-mucinous carcinoma (IPMC) of the pancreas with both carcinoma and osteosarcoma cells arising from IPMC cells

Jun Okamura,[1] Shigeki Sekine,[1] Satoshi Nara,[2] Hidenori Ojima,[1] Kazuaki Shimada,[2] Yae Kanai,[1] Nobuyoshi Hiraoka[1]

[1]Pathology Division, National Cancer Center Research Institute, Tokyo, Japan
[2]Division of Hepato-Biliary and Pancreatic Surgery, National Cancer Center Hospital, Tokyo, Japan

**Correspondence to**
Dr Nobuyoshi Hiraoka, Pathology Division, National Cancer Center Research Institute, 5-1-1 Tsukiji, Chuo-ku, Tokyo 104-0045, Japan; nhiraoka@ncc.go.jp

Accepted 9 October 2009

## ABSTRACT

Carcinosarcoma of the pancreas is extremely rare and its histogenesis is still unclear. This is a report on a 64-year-old female patient with an intraductal carcinosarcoma arising from intraductal papillary-mucinous carcinoma (IPMC) in the pancreas tail. The carcinosarcoma grew as a polypoid mass within the main pancreatic duct. Histologically, the tumour consisted of adenocarcinoma covering the luminal surface of the lesion with minimal stromal invasion, and osteosarcoma occupying the stroma. Immunohistochemical and gene mutation analyses revealed that both the carcinomatous and sarcomatous tumour cells of the carcinosarcoma, as well as the IPMC cells, expressed TP53 and had identical mutations in *KRAS* and *TP53* genes, indicating that these two neoplastic components of the carcinosarcoma shared a common tumorigenesis and arose from the IPMC. This is the first report of a carcinosarcoma originating in IPMC. These findings imply that carcinosarcoma with a heterologous mesenchymal component is of ductal origin.

## INTRODUCTION

Carcinosarcoma of the pancreas is a very rare tumour and only several cases have been reported hitherto.[1–6] These cases were diagnosed as carcinosarcoma histopathologically and immunohistochemically on the basis of the presence of both malignant epithelial and malignant mesenchymal components. Only two of the reported cases showed heterologous mesenchymal components.[1 2] The histogenesis of this tumour is still unclear, although there have been several hypotheses that it originates from epithelial cells, mesenchymal cells, undifferentiated precursor cells or stem cells. It has been difficult to assess its histogenesis, because pancreatic carcinosarcoma is extremely rare and is usually advanced at the time of diagnosis.

Here we present the first reported case of pancreatic intraductal carcinosarcoma with a heterologous mesenchymal component (osteosarcoma), which is located in an intraductal papillary-mucinous carcinoma (IPMC). This case is thought to be important for considering the histogenesis of pancreatic carcinosarcoma with a heterologous mesenchymal component.

## CASE REPORT

A 64-year-old Japanese woman who attended our hospital for a health check-up was found by abdominal ultrasonography to have a cystic tumour in the tail of the pancreas. She had no symptoms and all clinical and laboratory data were normal. The serum concentrations of tumour markers were elevated (CA19-9, 87 U/ml; carcinoembryonic antigen (CEA), 2.7 ng/ml). She had been treated for diabetes mellitus for 11 years. Abdominal CT revealed a 2 cm cystic mass in the pancreatic tail (figure 1A). Within the cyst, there were irregular and solid nodules with calculus. The tail of the pancreas had been totally replaced by the tumour. No lymphadenopathy, ascites, liver metastasis or mass in the soft tissues was found. Distal pancreatectomy was performed under a preoperative diagnosis of invasive carcinoma originating in IPMC. The operation was uneventful, and 12 months after surgery, the patient is well without any tumour recurrence or metastasis.

## PATHOLOGICAL AND GENETIC FINDINGS

A grossly elastic, hard, solid, spherical mass measuring 35×21×14 mm was present in the tail of the pancreas. At the cut surface, there was a papillary-to-polypoid projection located in the main and branch pancreatic ducts, which were cystically dilated and filled with clear yellowish mucinous fluid (figure 1B). These intraductal lesions were surrounded by yellowish-grey solid and nodular components of the tumour from the side of the pancreatic tail.

Histologically, the tumour comprised an intraductal neoplasm and a derivative invasive carcinoma (figure 2). The luminal surface of the dilated pancreatic ducts was covered with atypical mucin-secreting columnar epithelial cells showing papillary growth (figure 2A,B), indicating a diagnosis of IPMC. No ovarian-type stroma was evident. It was noteworthy that biphasic histological features were found in the polypoid lesion in the main pancreatic duct, which consisted of papillary proliferation of adenocarcinoma covering the luminal surface of the projecting mass with infrequent and minimal stromal invasion and an osteosarcoma occupying the stroma. The osteosarcoma showed invasive growth, but its extension was limited to the stroma of the IPMC, which was not beyond the duct wall



*J Clin Pathol* 2010;**63**:266–269. doi:10.1136/jcp.2009.071613

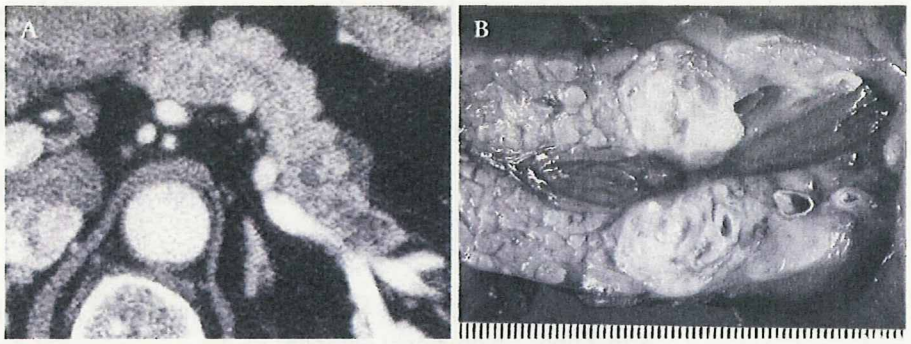


**Figure 1** (A) Abdominal CT image showing a 2 cm cystic mass in the pancreatic tail. (B) Fresh cut view of the body and tail of the pancreas.

(figure 2C–E). The osteosarcoma was characterised by a dense proliferation of malignant spindle-shaped and pleomorphic cells with mononucleated and multinucleated giant cells that had atypical and bizarre nuclei and formed osteoid and bone (figure 2E). Occasional infiltration of osteoclast-like multinucleated giant cells without nuclear atypia was evident. This intraductally proliferating mixed epithelial and mesenchymal tumour was diagnosed as carcinosarcoma, which seemed to have originated in the IPMC. Formation of osteoid and/or bone is rare but possible in cases of undifferentiated carcinoma with osteoclast-like giant cells, although the osteoid and/or bone is a result of reactive stromal metaplasia without any atypia in such cases.[7]

In addition to the intraductal tumour, IPMC cells had infiltrated beyond the duct wall and reached the surrounding stroma, showing a marked desmoplastic reaction at the side of the pancreatic tail bearing the tumour (figure 2B). The infiltrating cancer cells proliferated with poorly formed glands and solid to nested growth, indicating poorly differentiated adenocarcinoma. The infiltrating adenocarcinoma formed a nodular mass measuring 25×21×14 mm, although the invasive adenocarcinoma was not connected to the intraductal carcinosarcoma.

Immunohistochemical examination revealed expression of cytokeratins (AE1/AE3 and CK7) and vimentin, which

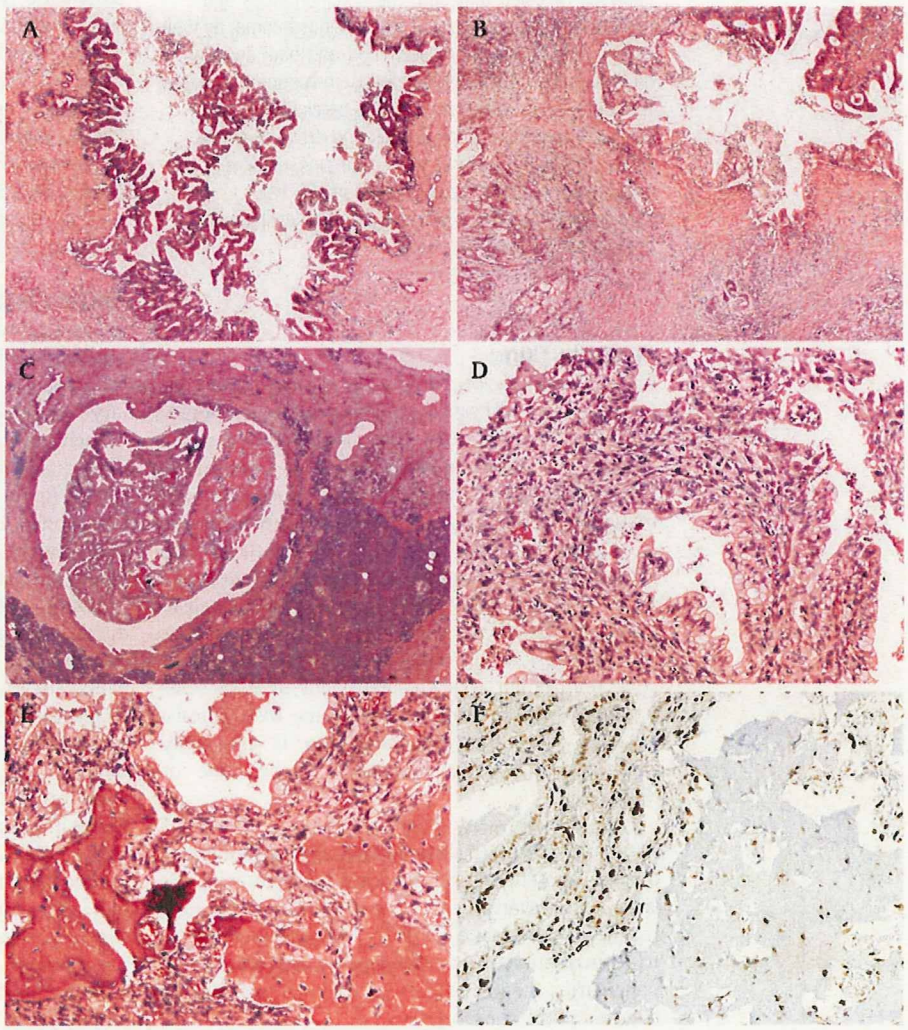


**Figure 2** (A, B) Histopathological features of intraductal papillary-mucinous carcinoma (IPMC) (A) and invasive adenocarcinoma arising from IPMC (B). (C–E) Histopathological features of intraductal carcinosarcoma originating in IPMC. (C) A very-low-power view of the polypoid lesion in the main pancreatic duct. (D, E) Mid-power view of the polypoid lesion. (F) Immunohistochemical expression of TP53 in intraductal carcinosarcoma originating in IPMC.

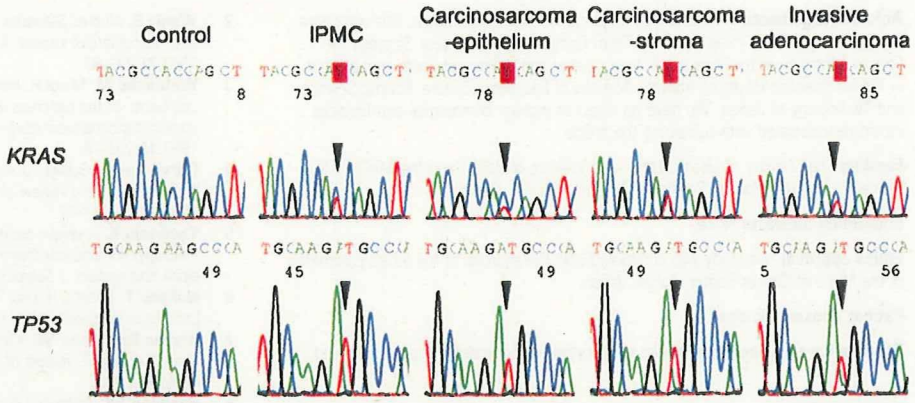


**Figure 3** Mutations of *KRAS* and *TP53* genes in each tumour component. All four tumour components examined (epithelial and mesenchymal tumour cells in the carcinosarcoma, intraductal papillary-mucinous carcinoma (IPMC) cells and invasive adenocarcinoma cells), harboured identical *KRAS* and *TP53* mutations. The sequences were read with reverse primers. Triangles indicate locations of point mutations.

confirmed the epithelial and mesenchymal components of tumour cells detected histologically. TP53 was expressed in the nuclei of most of the intraductal and invasive epithelial tumour cells as well as the mesenchymal tumour cells (figure 2F). CD68 antigen was expressed in some of the multinucleated giant cells without nuclear atypia. These CD68-positive osteolclast-like giant cells did not express TP53.

Four distinct tumour components (epithelial and mesenchymal tumour cells in the carcinosarcoma, IPMC cells and invasive adenocarcinoma cells) were separately laser-microdissected and analysed for *KRAS* and *TP53* mutations. DNA samples extracted from the microdissected tissues were subjected to PCR with a pair of specific primers to amplify exon 1 of *KRAS* or exon 4 of *TP53*, and isolated PCR products were sequenced bidirectionally. The analysis revealed identical *KRAS* (G35A mutation in exon 1) and *TP53* (T337A mutation in exon 4) mutations in all four tumour components examined (figure 3). Non-neoplastic pancreatic parenchyma adjacent to the tumour exhibited wild-type sequences, confirming the somatic nature of the mutations.

## DISCUSSION

Carcinosarcoma is a biphasic tumour consisting of an intimate admixture of malignant epithelial and mesenchymal components identifiable on the basis of their morphological, immunohistochemical and sometimes ultrastructural features. Nine cases of carcinosarcoma of the pancreas have been reported,[1–6] including two with heterologous mesenchymal components; one of the latter cases exhibited leiomyosarcoma, chondrosarcoma and rhabdomyosarcoma,[1] and the other showed malignant nerve sheath tumour as heterologous mesenchymal components.[2] No case of either carcinosarcoma arose from intraductal papillary-mucinous neoplasm (IPMN) and all were found at an advanced stage, with an average tumour diameter of 9.6 cm (range 2.5–19 cm).

To our knowledge, the present case of carcinosarcoma with a heterologous mesenchymal component originating in IPMN is the first of its kind to have been reported. Immunohistochemical and gene mutation analyses revealed that both the carcinomatous and sarcomatous tumour cells in the carcinosarcoma as well as the IPMC cells expressed TP53 and had common mutations in *KRAS* and *TP53* genes, indicating that these two neoplastic components of the carcinosarcoma had a common origin, IPMC. This case provides new findings supporting the hypothesis that carcinosarcoma with a heterologous mesenchymal component is of ductal origin and arises from IPMN.

The histogenesis of carcinosarcoma is still controversial, but the previously proposed hypotheses have now been combined as the following: (1) it is a combination tumour in which carcinomatous and sarcomatous elements arise from a multipotential stem cell; (2) it is a collision tumour in which two independent neoplasia, carcinoma and sarcoma, develop; (3) it is a carcinoma showing metaplastic changes to sarcoma components. The definition of carcinosarcoma in the WHO histological classification differs according to the organ in which the tumour develops. A mixed epithelial and mesenchymal tumour with heterologous mesenchymal components is defined as carcinosarcoma in the histological classification of tumours of many organs, including the colon and rectum, gallbladder and extrahepatic bile ducts, and lung.[8] In contrast, a mixed epithelial and mesenchymal tumour, regardless of the presence of heterologous mesenchymal components, is defined as carcinosarcoma in the histological classification of tumours of the breast and female genital tract. It is thought that most, but not all, of the mesenchymal components in carcinosarcoma of the female genital tract arise from the carcinoma through metaplastic change and that the small population of the carcinosarcoma left is formed by collision of carcinoma and sarcoma.[9] The present case suggests that carcinosarcoma of the pancreas arises from a carcinoma with metaplastic changes, although the WHO histological classification of pancreatic tumours includes no specific category for carcinosarcoma.[8] According to the previous report,[2] a sarcomatous component is speculated to arise from ovarian-type stroma characteristic of mucinous cystic neoplasm. In such a case, carcinosarcoma should be formed as a collision tumour.

In summary, we have presented a case of pancreatic intraductal carcinosarcoma originating in IPMC. Our morphological, immunohistochemical and genetic findings suggest that the carcinosarcoma with a heterologous mesenchymal component was ductal in origin.

### Take-home messages

- Carcinosarcoma of the pancreas is extremely rare and its histogenesis is still unclear.
- We describe an intraductal carcinosarcoma arising from intraductal papillary-mucinous carcinoma (IPMC) in the pancreas tail.
- Both the epithelial component (adenocarcinoma) and heterologous mesenchymal component (osteosarcoma) of the carcinosarcoma, as well as the IPMC, expressed TP53 and had identical mutations in *KRAS* and *TP53* genes, indicating that these two neoplastic components of the carcinosarcoma shared a common tumorigenesis and arose from the IPMC. These findings imply that carcinosarcoma with a heterologous mesenchymal component is of ductal origin.



*J Clin Pathol* 2010;**63**:266–269. doi:10.1136/jcp.2009.071613

**Acknowledgements** We thank Ms Rie Itoh for technical assistance. This work was supported by a Grant-in-Aid for Third Term Comprehensive 10-year Strategy for Cancer Control from the Ministry of Health, Labor and Welfare of Japan and a Grant-in-Aid for Scientific Research from the Ministry of Education, Culture, Sports, Science and Technology of Japan. We have no direct or indirect commercial and financial incentive associated with publishing the article.

**Funding** The Ministry of Health, Labor and Welfare of Japan and the Ministry of Education, Culture, Sports, Science and Technology of Japan.

**Competing interests** None.

**Ethics approval** This study was conducted with the approval of the ethics committee of the National Cancer Center, Tokyo, Japan.

**Patient consent** Obtained.

**Provenance and peer review** Not commissioned; not externally peer reviewed.

## REFERENCES

1. **Millis JM,** Chang B, Zinner MJ, *et al*. Malignant mixed tumor (carcinosarcoma) of the pancreas: A case report supporting organ-induced differentiation of malignancy. *Surgery* 1994;**115**:132–7.
2. **Wenig B,** Albores-Saavedra J, Buetow P, *et al*. Pancreatic mucinous cystic neoplasm with sarcomatous stroma: A report of three cases. *Am J Surg Pathol* 1997;**21**:70–80.
3. **Watanabe M,** Miura H, Inoue H, *et al*. Mixed osteoclastic/pleomorphic-type giant cell tumor of the pancreas with ductal adenocarcinoma: Histochemical and immunohistochemical study with review of the literature. *Pancreas* 1997;**15**:201–8.
4. **Darvishian F,** Sullivan J, Teichberg S, *et al*. Carcinosarcoma of the pancreas: A case report and review of the literature. *Arch Pathol Lab Med* 2002;**126**:1114–17.
5. **Yamazaki K.** A unique pancreatic ductal adenocarcinoma with carcinosarcomatous histology, immunohistochemical distribution of hCG-beta, and the elevation of serum alpha-feto-protein. *J Submicrosc Cytol Pathol* 2003;**35**:343–9.
6. **Nakano T,** Sonobe H, Usui T, *et al*. Immunohistochemistry and K-ras sequence of pancreatic carcinosarcoma. *Pathol Int* 2008;**58**:672–7.
7. **Hruban RH,** Pitman MB, Klimstra DS. eds. *AFIP Atlas of the Tumor Pathology Fourth Series Fascicle 6: Tumors of the Pancreas*. Washington, DC: American Registry of Pathology, 2007.
8. **Hamilton SR,** Aaltonen LA, eds. *Pathology and genetics. Tumours of the digestive system. World Health Organization Classification of Tumours*. Lyon, France: IARC Press, 2000.
9. **McCluggage WG.** Malignant biphasic uterine tumors: carcinosarcomas or metaplastic carcinomas? *J Clin Pathol* 2002;**55**:321–5.

Cancer Science
The official journal of the Japanese Cancer Association JCA

# Fibroblast growth factor receptor 3 mutation in voided urine is a useful diagnostic marker and significant indicator of tumor recurrence in non-muscle invasive bladder cancer

Makito Miyake,[1,8] Kokichi Sugano,[1,9] Hitomi Sugino,[1] Kazuho Imai,[1] Eri Matsumoto,[1] Koshi Maeda,[2] Shinich Fukuzono,[2] Hiroki Ichikawa,[3] Kiyotaka Kawashima,[3] Kaoru Hirabayashi,[4] Tetsuro Kodama,[5] Hiroyuki Fujimoto,[6] Tadao Kakizoe,[6] Yae Kanai,[7] Kiyohide Fujimoto[8] and Yoshihiko Hirao[8]

[1]Oncogene Research Unit/Cancer Prevention Unit, Tochigi Cancer Center Research Institute, 4-9-13 Yonan, Utsunomiya; [2]Hitachi High-Technologies Corporation, Hitachinaka, Ibaraki; [3]Department of Urology, [4]Department of Clinical Laboratory, [5]Director, Tochigi Cancer Center Hospital, Utsunomiya, Tochigi; [6]Department of Urology, National Cancer Center Hospital, [7]Pathology Division, National Cancer Center Research Institute, Tokyo; [8]Department of Urology, Nara Medical University, Kashihara, Nara, Japan

(Received May 06, 2009/Revised August 17, 2009/Accepted August 23, 2009/Online publication October 14, 2009)

**The fibroblast growth factor receptor (FGFR)-3 gene encodes a receptor tyrosine kinase that is frequently mutated in non-muscle invasive bladder cancer (NMIBC). A sensitive and quantitative assay using peptide nucleic acid-mediated real-time PCR was developed for detecting *FGFR3* mutations in the urine samples and evaluated as a molecular marker for detecting intravesical recurrence of NMIBC in patients undergoing transurethral resection of bladder tumor. *FGFR3* mutation was examined in tumor tissues and serially taken pre- and postoperative urine sediments in 45 NMIBC patients with a median follow up of 32 months. *FGFR3* mutations were detected in 53.3% (24/45) of primary tumor tissues, among which intravesical recurrence developed in 37.5% (9/24) of cases. *FGFR3* mutation in the primary tumor was not a significant prognostic indicator for recurrence, while the proportion of *FGFR3* mutation (i.e. tumor cellularity was ≥11%) in the preoperative urine sediments was a significant indicator for recurrence in patients with *FGFR3* mutations in the primary tumors. *FGFR3* mutations were detected in 78% (7/9) of postoperative urine samples from recurrent cases with *FGFR3* mutations in the tumor, while no mutations were detected in the urine of 15 non-recurrent cases. Urine cytology was negative in all cases with *FGFR3* mutations in the primary tumors, while the sensitivity of cytological examination was as high as 56% (5/9) in cases showing wild-type *FGFR3* in the primary tumors. Urine *FGFR3* mutation assay and cytological examination may be available in the future as complementary diagnostic modalities in postoperative management of NMIBC. (*Cancer Sci* 2010; 101: 250–258)**

Urothelial carcinoma (UC) is a histological subtype accounting for more than 90% of all bladder cancers, and there are 357 000 new cases every year worldwide.[1] Bladder UCs are generally divided into two groups for clinical management, depending on the pathological stage. Most of the newly diagnosed UCs are non-muscle invasive bladder cancer (NMIBC; i.e., pTa or pT1), and the initial treatment is transurethral resection of bladder tumor (TURBT). After the initial TURBT, the patients undergo intensive surveillance by cystoscopic examination at regular intervals; usually every 3 months, because up to 70% of these patients will experience intravesical recurrence, and 10–30% of the lesions will progress to life-threatening muscle-invasive disease (≥pT2).[2] Cystoscopy is an inconvenient, invasive, and expensive diagnostic modality, but currently it is the gold standard for detecting intravesical recurrence in the postoperative follow up. Although urine bound diagnostic tests including urinary cytology, nuclear matrix protein (NMP)22, and bladder tumour antigen (BTA) tests are used in the management after TURBT or bladder cancer screening, their usefullness is limited due to their poor sensitivity or specificity.[3] In previous reports, various molecular markers detectable in urine have been considered as a useful and non-invasive clinical assay improving the sensitivity of conventional tests.[4–10] In urine-based detection assays, contamination with normal urothelium or leucocytes can mask the signals of targeted somatic mutations.[11]

Fibroblast growth factor receptor (FGFR)-3 belongs to a family of structurally related tyrosine kinase receptors (FGFR1–4), and plays important roles in many biological processes including embryogenesis, proliferation, differentiation, and angiogenesis.[12] Recent reports have demonstrated that constitutively activated *FGFR3* mutations exist in more than 50% of primary bladder UC.[13] *FGFR3* mutations are especially prevalent in the low-grade papillary tumors (pTa/G1), but they are infrequent in high-grade or high-stage UC.[13,14] *FGFR3* mutation in urine sediments may be a suitable biomarker for detection of low-grade and low-stage UC. Previous studies revealed that mutation of *FGFR3* in the voided urine can be detected at high sensitivity in patients with *FGFR3*-mutated bladder UC.[15–17] However, there is no report validating the feasibility and usefulness of detecting *FGFR3* mutation in the voided urine samples by serial determinations during follow up after TURBT. Recently, we have reported an assay protocol for detecting *FGFR3* mutations in bladder tumor tissues and urine sediments by peptide nucleic acid (PNA)-mediated real-time PCR clamping assay.[17] In PNA-mediated PCR clamping, PNA is designed to anneal to a wild-type DNA sequence and inhibits the annealing of PCR primer to the wild-type alleles, resulting in preferential amplification of the mutated alleles. With 50 ng of genomic DNA as a template, this method allows sensitive and quantitative detection of the *FGFR3* mutations in mutational hotspots in exons 7, 10, and 15 in bladder cancer. In the present study, we modified the protocol of the PNA-mediated PCR clamping assay to achieve quantitative detection of the *FGFR3* mutations present in the urine samples at a concentration of 1% in only 1 ng of genomic DNA available as a template for PCR. With this the revised protocol, we assessed the usefulness of *FGFR3* mutations as a

[9]To whom correspondence should be addressed.
E-mail: ksugano@tcc.pref.tochigi.lg.jp



doi: 10.1111/j.1349-7006.2009.01334.x

diagnostic modality in the voided urine samples for the postoperative management of NMIBC. This is considered the first report addressing the significance of *FGFR3* mutations in preoperative urine sediments as a novel indicator predicting the risk of intravesical recurrence of NMIBC.

## Materials and Methods

**Subjects and collection of the tumor tissues and voided urine samples after the initial TURBT.** The patients undergoing TURBT from April 2002 through March 2005 at the Departments of Urology at Tochigi Cancer Center Hospital and Nara Medical University Hospital were enrolled in this study. All participants had received study information and signed a written informed consent form. The voided urine samples before the initial TURBT were taken from the patients. The resected tumors were examined histologically and staged and graded according to the 2002 TNM classification and the 1973 World Health Organization (WHO) classification systems, respectively.[18,19] A total of 45 subjects with NMIBC were eligible for the study and were followed up until the histological diagnosis of tumor recurrence or up to 3 years postoperatively by routine cystoscopy and urine cytological examination. The median follow-up period was 32 months (range 4–36 months). The patients were monitored by routine cystoscopy and urine cytology at 1, 3, 6, 9, 12, 15, 18, 21, 24, 30, and 36 months after the initial TURBT. Intravesical recurrence was confirmed by histological diagnosis of tumor tissues obtained during TURBT for recurrence. The voided urine samples were divided and subjected to urine cytology and DNA extraction for gene testing. The urine samples were stored at −20°C until DNA extraction.

**DNA extraction and measurement of DNA concentration.** DNA extraction from the tumor tissues and peripheral blood lymphocytes (PBL) was carried out as described previously.[6] DNA extraction from the urine samples was carried out with the QIAamp DNA Blood Mini Kit (Qiagen, Valencia, CA, USA) according to the manufacturer's instructions. Briefly, the urine sample in a 50-mL tube was centrifuged at 180*g* for 5 min. The cell pellet was digested by Qiagen protease and subjected to DNA extraction by column centrifugation. In the final step, DNA was eluted from the column in 150 μL of the elution buffer. The genomic DNA concentration was determined by ultraviolet measurement using an ND-1000 spectrophotometer (NanoDrop Technologies, Wilmington, DE, USA). For analysis of samples with DNA concentrations less than 50 ng/μL, DNA concentration was quantified by real-time PCR using LightCycler (Roche Diagnostics, Mannheim, Germany). Quantification was carried out with the same primer pairs used for PNA-mediated real-time PCR clamping for amplification of *FGFR3* exon 7.[17] Serially diluted assay standards were prepared by adjusting the genomic DNA concentrations to 100, 10, 1, and 0.1 ng/μL. DNA samples and assay standards were subjected to real-time PCR in a 20-μL reaction volume containing genomic DNA, 10 picomole of each primer, and 10 μL of QuantiTect PCR master mix (Qiagen) containing SYBR Green I dye. The conditions of real-time PCR are described in Table 1. DNA concentration was calculated from the crossing points (CP) of the assay standards and samples according to the fit points method on LightCycler Data Analysis software version 3.5 (Roche Diagnostics corporation).

**PNA-mediated pre-main amplifier method for the low-copy number DNA template.** Previously, we reported a PNA-mediated real-time PCR clamping assay for detection of *FGFR3* mutations.[17] This method enabled sensitive and reproducible detection of *FGFR3* mutations in cases where 50 ng of genomic DNA were available as the template for PCR. In the PNA-mediated PCR-clamping, the chance of nucleotide misincorporation to the PNA binding sequence increases in reverse correlation with the amount of template DNA. When the amount of template DNA was 1 ng in genomic DNA (equivalent to 300 copies), mutations were hardly distinguishable from those caused by misincorporation of dNTPs. To overcome this pitfall, we modified the assay protocol to detect *FGFR3* mutations at a concentration of 1% (three copies) in 1 ng (300 copies) of the template genomic DNA. We called the newly established method as PNA-mediated pre-main amplifier (PPA), which consisted of two steps of amplification (Fig. 1). Low-copy number DNA template was amplified by the pre-amplifier step and then set on the main amplifier to perform the PNA-mediated real-time PCR clamping. Pre-amplification was carried out in a PCR tube using DNA Engine Dyad Thermal Cycler (MJ Research, Watertown, MA, USA) in 20-μL aliquots consisting of 1 ng of genomic DNA, 10 μL of QuantiTect PCR master mix, and 10 picomole of each primer. The sequences of primer pairs were as reported previously.[17] Conditions of the thermal cycling in the pre-amplifier step were as follows: denaturing at 95°C for 15 min, amplification of seven cycles consisting of heat denaturation at 94°C for 15 s, annealing at 64°C (exon 7), 58°C (exon 10), and 60°C (exon 15) for 20 s, and extension at 72°C for 20 s. After final cooling to 4°C, 5 μL of the solution containing 2.5 μL of QuantiTect PCR master mix and 2.5 μL of PNA solution were added and mixed by gentle pipetting. The sequences of PNA and the final concentrations are listed in Table 1. Of 25 μL of the mixed solution, 20 μL was transferred to a capillary tube for the LightCycler and set on the main amplifier performing the real-time PCR (Table 1). CP of PPA were determined by the fit points method.

**Detection of *FGFR3* mutations in the tumor tissues and urine samples.** The assay standards for mutation analysis of each exon were prepared as described previously.[17] In the clinical

**Table 1. Sequences of PCR primers and peptide nucleic acid (PNA), and PCR conditions**

| Real-time PCR | Sequence of primers and PNA | PNA concentration (μM) | Cycle no. | PNA binding step (°C) | Annealing step (°C) |
|---|---|---|---|---|---|
| DNA quantification | 5′-TGA GCG TCA TCT GCC CCC ACA GAG-3′ (sense)<br>5′-GGG CCC ACC TTG CTG CCA TTC A-3′ (antisense) | – | 45 | – | 64 |
| Main amplifier for exon 7 | 5′-TGA GCG TCA TCT GCC CCC ACA GAG-3′ (sense)<br>5′-GGG CCC ACC TTG CTG CCA TTC A-3′ (antisense)<br>H2N-AGC GCT CCC CGC ACC-N2H (PNA) | 0.4 | 45 | 72 | 64 |
| Main amplifier for exon 10 | 5′-CCA GGC CTC AAC GCC CAT GTC TTT-3′ (sense)<br>5′-ACC CCG TAG CTG AGG ATG CCT GCA-3′ (antisense)<br>H2N-CAT ACA CAC TGC CCG C-N2H | 1 | 45 | 67 | 58 |
| Main amplifier for exon 15 | 5′-GCA ATG TGC TGG TGA CCG AG-3′ (sense)<br>5′-CGG GCT CAC GTT GGT CGT CT-3′ (antisense)<br>H2N-GGT CGT CTT CTT GTA GT-N2H | 2 | 45 | 70 | 60 |

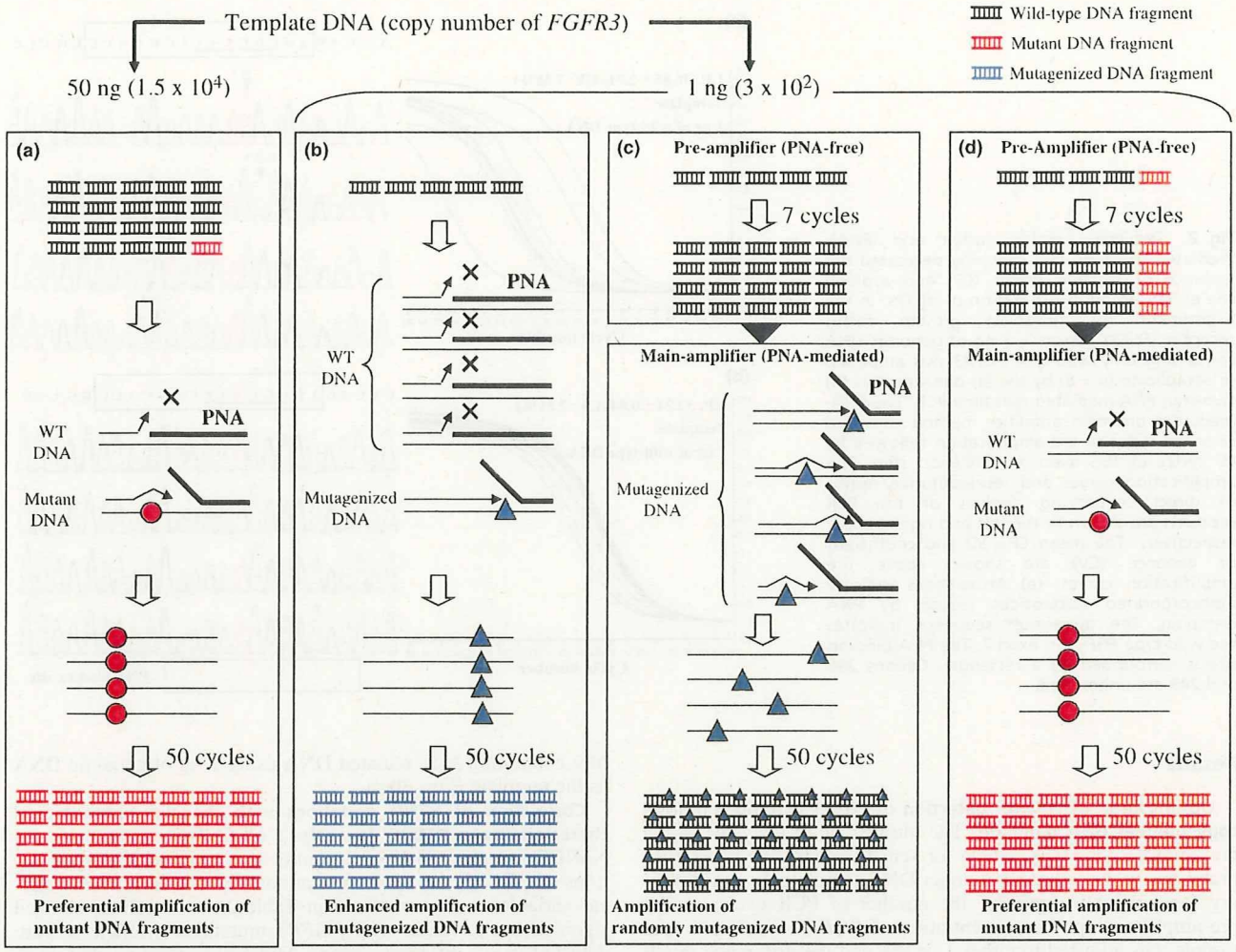


**Fig. 1.** Schematic diagram of the one-step and two-step peptide nucleic acid (PNA)-mediated PCR clamping. The feasibility of PNA-mediated PCR clamping was highly influenced by the amount of the template DNA. (a) Fifty nanograms of genomic DNA containing a low proportion of mutated DNA was used as a template. PNA-mediated PCR enabled preferential amplification of the mutated DNA, leading to enrichment of the mutated DNA fragments. The red circle indicates a mutated DNA sequence. (b) One nanogram of genomic DNA containing only wild-type DNA was used as the template. Misincorporation of dNTPs occurred in the sequences of the PNA-binding site, due to a failure in DNA synthesis brought about by DNA polymerase. When the nucleotide misincorporation (blue triangle) occurred in the early cycles of PNA-mediated PCR, a mutagenized sequence was subjected to subsequent amplification. (c) One nanogram of the template DNA containing only wild-type DNA was used for the PNA-free pre-amplifier step prior to the PNA-mediated main-amplifier. Seven PCR cycles of the pre-amplifier step generated sufficient copies of fibroblast growth factor receptor (*FGFR*)-3 DNA fragments, which were used as the template for the main-amplifier. The PNA-mediated reaction produced a randomly mutagenized DNA sequence that could slip from PNA clamping. However, all of these mutagenized fragments resulted in dispersion of mutagenesis signals and were scarcely detectable in the direct sequencing analysis. (d) One nanogram of genomic DNA with a low proportion of mutant DNA was used as the template. The PNA-free pre-amplifier increased the copy numbers of the *FGFR3* molecules as a whole, leading to a successful preferential amplification of the mutated DNA fragments in the main-amplifier. The black, red, and blue fragments indicate the wild-type, mutated, and mutagenized DNA fragments, respectively.

samples with DNA concentrations of ≥50 ng/μL, mutation analyses were carried out according to the one-step assay using 50 ng of genomic DNA as the template.[17] In the samples with DNA concentrations ranging from 0.125 to 50 ng/μL, a modified protocol was adapted using 1 ng of genomic DNA as the template. In each run, we defined CP of the assay standard corresponding to 1% tumor cellularity as the minimal detectable dose for *FGFR3* mutations. Accordingly, a sample showing CP less than that of the 1% assay standard was considered mutation positive and subjected to direct sequencing to identify the mutational types.[17] The tumor cellularities of the mutation-positive samples were determined by a regression analysis using a standard curve obtained from 100, 10, and 1% assay standards. The samples with DNA concentrations less than 0.125 ng/μL were regarded as unavailable samples unless they could be enriched in DNA concentration.

**Statistical analysis.** Statistical analyses and drawing figures were done using PRISM software version 4.00 (GraphPad Software, Inc., San Diego, CA, USA). Student's *t*-test, Chi-square test, and Fisher's exact test were used to analyze the correlations between the clinicopathological variables and *FGFR3* mutational status in the primary tumors. Recurrence-free survival curves were plotted according to the Kaplan–Meier method, and the log-rank test was applied for statistical significance. A receiver operating characteristic (ROC) curve was used to define the optimal cut-off value of tumor cellularity in the urine sediments. The non-parametric variables were analyzed by the Mann–Whitney *U*-test. A *P*-value of $<0.05$ was considered significant.


doi: 10.1111/j.1349-7006.2009.01334.x

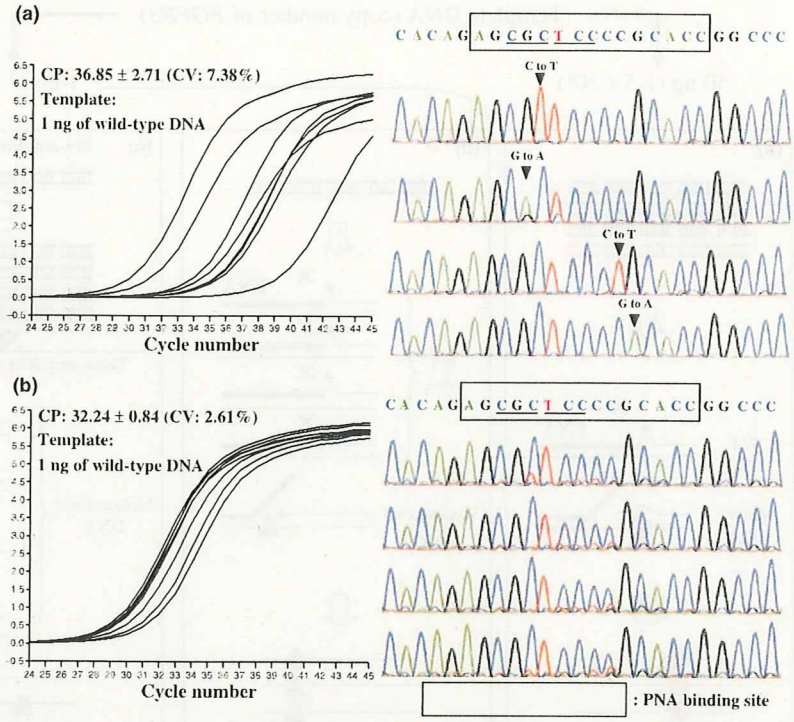


**Fig. 2.** Two-step peptide nucleic acid (PNA)-mediated real-time PCR clamping decreased the variance of crossing points (CP) and avoided the enhanced misincorporation of dNTPs. In the experiment for fibroblast growth factor receptor (*FGFR*)-3 exon 7, 1 ng of genomic DNA containing only wild-type *FGFR3* was amplified in octaplicate ($n$ = 8) by the (a) one-step and (b) two-step PNA-mediated real-time PCR. The PNA-mediated pre-main amplifier method consisted of seven cycles of pre-amplification followed by 45 cycles of the main amplification step. The amplification curves and representative results of direct sequencing analysis of the PCR products are shown in the left and right panels, respectively. The mean CP ± SD and coefficient of variance (CV) are shown above the amplification curves. (a) Arrowheads indicate disincorporated nucleotides caused by PNA clamping. The uppermost sequence indicates the wild-type *FGFR3* in exon 7. The PNA binding site is surrounded by a rectangle. Codons 248 and 249 are underlined.

## Results

**Optimization of PPA for detection of *FGFR3* mutations in low-copy number DNA template.** The number of PCR cycles in the pre-amplifier step was critical for sensitive detection of *FGFR3* mutations in the low-copy number DNA template. In a preliminary experiment to optimize the number of PCR cycles in the pre-amplifier step, the concentration of *FGFR3* mutation in the sample was adjusted to either 1 or 0% and the difference in CP was maximal when seven cycles of PCR were used in the pre-amplification step ($P$ = 0.001). In this condition, we compared the coefficients of variation (CV) between the one-step and two-step assays using 1 ng of wild-type genomic DNA as the template (Fig. 2a,b left). The assay CV of CP in the PPA method was much smaller than that of the one-step assay (2.61 vs 7.38%, respectively). The sequencing analysis of the amplified DNA fragments in the one-step assay revealed point mutations caused by nucleotide misincorporation virtually in all samples (Fig. 2a right), whereas those amplified by the PPA assay showed no recognizable mutations except for a slight increase in the background signals. These results indicated that the PPA method circumvented the chance of a nucleotide misincorporation and minimized the CV of the CP for wild-type DNA or 0% standard (Fig. 2b right). In this condition, the assay standards with 100, 10, and 1% mutations in exon 7 of *FGFR3* and 0% (wild type) were amplified by the PPA method using 1 ng of DNA template, and the results were compared with those of the one-step assays. The CPs of the assay standards were statistically significant between each other (Fig. 3a) and direct sequencing analysis of the 1% standard revealed that all of eight samples showed S249C mutation (TCC → TGC) in exon 7. These results demonstrated that the mutations were reliably detected in the samples containing ≥1% mutated DNA using only 1 ng of DNA template, and that the PPA method overcame the limitation of our prior study.

In analysis of exons 10 and 15, seven amplification cycles in the pre-amplifier step were used to detect mutations in the samples containing ≥1% mutated DNA using 1 ng of genomic DNA as the template (Fig. 3b,c).

**Correlation of *FGFR3* mutations with the clinicopathological characteristics in NMIBC.** In analysis of *FGFR3* mutations in 45 NMIBC samples, 24 (53.3%) tumors harbored activating mutations of *FGFR3*, and their correlations with the clinicopathological variables are summarized in Table 2. No variables showed significant correlation with *FGFR3* mutations. Mutations were detected in six different codons. Mutations affecting the extracellular domain (exon 7) or transmembrane domain (exon 10) accounted for 95.8% (23/24) (Table 3). Intravesical recurrence was detected in 18 of 45 subjects (40%). The clinicopathological variables of the primary tumors, such as tumor stage, histological grade, tumor size, multiplicity, presence of carcinoma *in situ* lesion, and *FGFR3* mutational status, did not correlate with the intravesical recurrence (Table 4).

**Clinical usefulness of detecting *FGFR3* mutation in the urine sediments.** A total of 429 voiding urine samples were taken from 45 cases, among which 61 samples were preoperative urine samples consisting of 35 from recurrent and 26 from non-recurrent cases (Table 5). The remaining 368 urine samples were obtained serially during follow up, among which 93 samples were from recurrent cases and 275 samples were from non-recurrent cases. The concentrations of genomic DNA extracted from the urine samples were quantified in all samples prior to the assay. Of 429 urine samples, 114 (26.6%) were not available for the assay because their DNA concentrations were <0.125 ng/μL. A total of 315 samples (73.4%) were subjected to the *FGFR3* mutation detection assay. They were subjected to either the conventional PNA-mediated real-time PCR clamping assay or PPA method depending on their DNA concentrations.

**Risk of intravesical recurrence in patients showing *FGFR3* mutation in tumor tissues and urine sediments.** In 21 of 24 cases with *FGFR3* mutation in primary tumors, genomic DNA samples extracted from preoperative urine sediments before the initial TURBT were available for mutation detection assay. The sensitivity of *FGFR3* mutation in the urine samples was 62%

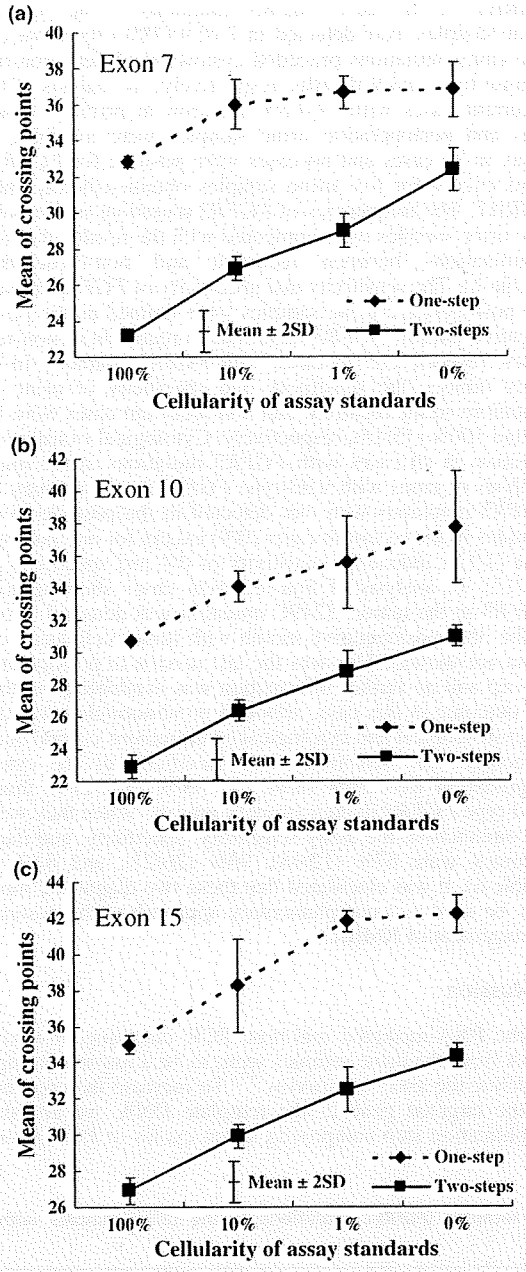


**Fig. 3.** Validation for sensitive detection of fibroblast growth factor receptor (*FGFR*)-3 mutation in trace amounts of the template DNA. (a) One nanogram of genomic DNA of four assay standards with 0, 1, 10, and 100% of tumor cellularity was amplified in octaplicate samples ($n$ = 8) under the conditions of the two-step assays comprising seven amplification cycles of the peptide nucleic acid (PNA)-free pre-amplifier, followed by PNA-mediated real-time PCR clamping for exon 7 of the *FGFR3* gene (solid lines). The data from the one-step assay are shown for comparison (dashed lines). The mean crossing points (CP) are plotted and the error bars represent 2 SD. Similar experiments were carried out to validate the assay protocols for (b) exon 10 and (c) exon 15.

(13/21), and their mutational types coincided with those of the primary tumors in all cases. In 21 cases showing wild-type *FGFR3* in primary tumor tissues, the preoperative urine samples were available for the assay in 13 cases and no mutations were found in these samples, showing the specificity of 100% (0/13). Tumor cellularities in the preoperative urine sediments were significantly higher in the recurrent cases than in the non-recurrent cases (Fig. 4a; $P$ = 0.008). An ROC curve analysis was performed to define the optimal cut-off value of tumor cellularity in the preoperative urine sediments. The area under the curve (AUC) was 0.847 (95% confidence interval, 0.669–1.026), and the cut-off value with optimal sensitivity and specificity was defined as 11% (Fig. 4b).

*FGFR3* mutational status in the primary tumors was not a significant predictor of intravesical recurrence after TURBT

**Table 2. Clinicopathological characteristics and fibroblast growth factor receptor (*FGFR*)-3 mutation status**

| Variables | Total | *FGFR3* status | | % of mutation | *P*-value |
|---|---|---|---|---|---|
| | | Wild-type | Mutation | | |
| Age (years) | | | | | |
| Mean ± SD | 63.0 ± 11.2 | 63.1 ± 12.7 | 62.8 ± 9.6 | – | 0.98 |
| Range | 36–80 | 36–80 | 45–78 | – | |
| Sex | | | | | |
| Male | 35 | 15 | 20 | 57 | 0.27 |
| Female | 10 | 6 | 4 | 40 | |
| Smoking history | | | | | |
| Present | 29 | 11 | 18 | 62 | 0.11 |
| Absent | 16 | 10 | 6 | 38 | |
| Tumor size (diameter, cm) | | | | | |
| <1 | 10 | 4 | 6 | 60 | 0.73 |
| 1–3 | 25 | 13 | 12 | 48 | |
| 3< | 10 | 4 | 6 | 60 | |
| Multiplicity | | | | | |
| Solitary | 27 | 12 | 15 | 56 | 0.71 |
| 2–3 | 12 | 5 | 7 | 58 | |
| ≥4 | 6 | 4 | 2 | 33 | |
| Pathological stage | | | | | |
| pTa | 19 | 7 | 12 | 63 | 0.26 |
| pT1 | 26 | 14 | 12 | 46 | |
| Tumor grade | | | | | |
| G1 | 6 | 3 | 3 | 50 | 0.97 |
| G2 | 35 | 16 | 19 | 54 | |
| G3 | 4 | 2 | 2 | 50 | |
| Concomitant CIS | | | | | |
| Present | 3 | 2 | 1 | 33 | 0.45 |
| Absent | 42 | 19 | 23 | 55 | |
| BCG therapy | | | | | |
| No | 40 | 19 | 21 | 53 | 0.87 |
| Treated | 5 | 2 | 3 | 60 | |
| Total | 45 | 21 | 24 | 53 | |

BCG, Bacille Calmette Guerin; CIS, carcinoma *in situ*.

**Table 3. Fibroblast growth factor receptor (*FGFR*)-3 mutational types detected in this study**

| *FGFR3* | Mutational type | | *n* | % |
|---|---|---|---|---|
| | Codon | Nucleotide | | |
| Exon 7 | R248C | CGC → TGC | 4 | 16.7 |
| | S249C | TCC → TGC | 8 | 33.3 |
| Exon 10 | G372C | GGC → TGC | 1 | 4.2 |
| | S373C | AGC → TGC | 1 | 4.2 |
| | Y375C | TAT → TGT | 9 | 37.5 |
| Exon 15 | K652E | AAG → GAG | 1 | 4.2 |
| Total | | | 24 | 100 |



doi: 10.1111/j.1349-7006.2009.01334.x

**Table 4. Correlation of the stage, histological grade, tumor size, multiplicity, concomitant CIS and fibroblast growth factor receptor (*FGFR*)-3 mutations in the tissue with intravesical tumor recurrence**

| Variables | Total | Recurrent | Non-recurrent | *P*-value* |
|---|---|---|---|---|
| No. subjects | 45 | 18 | 27 | |
| Stage | | | | |
| pTa | 19 | 8 | 11 | 1.00 |
| pT1 | 26 | 10 | 16 | |
| Grade | | | | |
| G1 | 6 | 1 | 5 | 0.43 |
| G2 | 35 | 15 | 20 | |
| G3 | 4 | 2 | 2 | |
| Tumor size (cm) | | | | |
| <3 | 35 | 12 | 23 | 0.14 |
| ≥3 | 10 | 6 | 4 | |
| Multiplicity | | | | |
| Solitary | 27 | 10 | 17 | 0.45 |
| Multiple | 18 | 8 | 10 | |
| Concomitant CIS | | | | |
| Absent | 42 | 16 | 26 | 0.25 |
| Present | 3 | 2 | 1 | |
| *FGFR3* mutations in the tumor tissues | | | | |
| Wild-type | 21 | 9 | 12 | 0.89 |
| Mutation | 24 | 9 | 15 | |

CIS, carcinoma *in situ*; *logrank test.

(Table 4). In cases harboring *FGFR3* mutations in the primary tumor, the levels of *FGFR3* mutations in the preoperative urine sediments significantly correlated with the 3-year recurrence-free survival rates (83.3 vs 22.2%) (Fig. 4c), whereas the results of preoperative urine cytology did not correlate with the recurrence-free survival.

**Serial determination of *FGFR3* mutations in the voided urine samples during the follow-up period after the initial TURBT.** *FGFR3* mutations in serially obtained urine samples were assayed quantitatively in the postoperative follow-up period. Low-copy number DNA samples were amplified by the PPA method using 1 ng of genomic DNA as the template. In 21 cases harboring *FGFR3* mutations in primary tumors, assay results were plotted on a 3-D line chart (Fig. 5). The preoperative sensitivities of urine *FGFR3* mutations in the recurrent and non-recurrent cases were 88.9% (8/9) and 41.7% (5/12), respectively. *FGFR3* mutations were not detected 1 month after the initial TURBT in all cases. *FGFR3* mutations in the postoperative urine samples were detected in 7 of 9 (78%) recurrent cases. In two cases, mutations preceded cystoscopical detection of tumor relapse by 6 and 9 months, respectively. In analysis of the non-recurrent cases with *FGFR3* mutation in primary tumors, the pre- and postoperative urine samples were available for the assay in 12 cases and no cases were positive for *FGFR3* mutations except for five urine samples obtained before the initial TURBT. The frequencies of *FGFR3* mutations in the postoperative urine samples were compared with the results of cytological examinations between recurrent and non-recurrent cases (Table 6). The sensitivity and specificity of *FGFR3* mutations in the postoperative urine samples were defined as the positive or negative rates of *FGFR3* mutations in recurrent or non-recurrent cases, respectively. In cases with *FGFR3* mutation in the primary tumors, the sensitivity and specificity of urine *FGFR3* mutations in the recurrent and non-recurrent cases were 78% (7/9) and 100% (15/15), respectively. Cytological examination was negative in all cases with *FGFR3* mutations in the tumors. In analysis of cases with wild-type *FGFR3* in the primary tumors, *FGFR3* mutations were not detected in the postoperative urine samples in the recurrent cases (0/9) except for one non-recurrent case (1/12), indicating sensitivity of 0% and specificity of 92% (11/12). In analysis of non-recurrent cases showing wild-type *FGFR3* in the tumor, S249C mutation was detected in one case at the 36th postoperative month with tumor cellularity of 2.1% (data not shown). This was the last session in postoperative follow up and no further information was available as to the clinical outcome in this case, although no abnormality was detected by cystoscopical and cytological examinations carried out simultaneously. The sensitivity and specificity of the cytological examination were 56% (5/9) and 100% (12/12) in those with wild-type *FGFR3* in their primary tumors. When they were used in combination, the assay sensitivity, specificity, and diagnostic accuracy were 67% (12/18), 96% (26/27), and 84% (38/45) (Table 6). It was elucidated that these two diagnostic modalities may be used as a complementary approach to the postoperative management of NMIBC.

## Discussion

In the PNA-mediated real-time PCR clamping, low yields of DNA from the urine samples seem to be a major limiting factor to define the assay sensitivity.[17] To increase the copy numbers of the targeted gene in the template DNA, we added a pre-amplification step comprising seven cycles of PCR prior to the

**Table 5. Correlation of DNA concentration and fibroblast growth factor receptor (*FGFR*)-3 mutations in the urine samples with tumor recurrence**

| Variables | Total | Recurrent | Non-recurrent | *P*-value |
|---|---|---|---|---|
| Collected urine samples | 429 | 128 | 301 | |
| Preoperative | 61 | 35† | 26 | |
| Follow-up | 368 | 93 | 275 | |
| DNA concentration (ng/μL) | | | | |
| Total | | | | |
| 50≦ | 83 (19.3%) | 23 (18.0%) | 60 (19.9%) | 0.885 |
| 0.125–50 | 232 (54.1%) | 71 (55.5%) | 161 (53.5%) | |
| 0.125< | 114 (26.6%) | 34 (26.6%) | 80 (26.6%) | |
| Mean ± SD (ng/μL) | 53.8 ± 187.6 | 36.2 ± 98.1 | 61.6 ± 214.3 | |
| Detection of *FGFR3* mutation in urine sediments | | | | |
| No. samples available for the assay | 315 | 94 | 221 | |
| Mutated | 26 (8.3%) | 20 (21.3%) | 6 (2.7%) | <0.0001 |
| WT | 289 (91.7%) | 74 (78.7%) | 215 (97.3%) | |

†Preoperative urine samples consisted of samples obtained in the initial transurethral resection of bladder tumor ($n$ = 18) and transurethral resection of bladder tumor for recurrence ($n$ = 17).

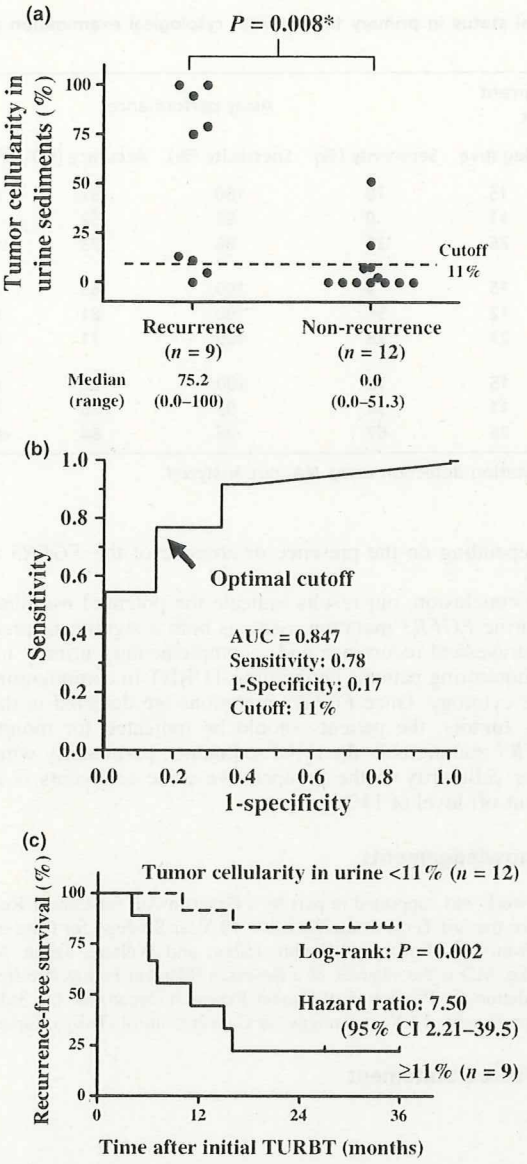


Fig. 4. The tumor cellularity in the preoperative urine predicted the risk of intravesical recurrence in patients with fibroblast growth factor receptor (*FGFR*)-3-mutated bladder urothelial carcinoma (UC). (a) The tumor cellularities in the preoperative urine sediments were plotted in the recurrent ($n$ = 9) and non-recurrent ($n$ = 12) groups of 21 cases with *FGFR3*-mutated bladder UC. The dashed line indicates the optimal cut-off point (≥11% and <11%) as determined with receiver operating characteristic (ROC) curve analysis shown in (b); *Mann–Whitney *U*-test. (b) A receiver operating characteristic curve was generated to define the optimal cut-off value of tumor cellularity in the preoperative urine sediments. The optimal cut-off value for predicting the intravesical recurrence was defined as the point closest to the upper-left corner of the graph (black arrow). (c) Recurrence-free survival curves according to the cut-off value (≥11% and <11%) of tumor cellularity in the preoperative urine sediments are shown. AUC, area under the curve; CI, confidence interval.

PNA-mediated real-time PCR clamping. This modified assay protocol achieved a sensitive method detecting *FGFR3* mutations at concentrations of ≥1% in 1 ng of the template DNA. One nanogram of genomic DNA with 1% of *FGFR3* mutations corresponds to as few as three copies of mutated *FGFR3*.

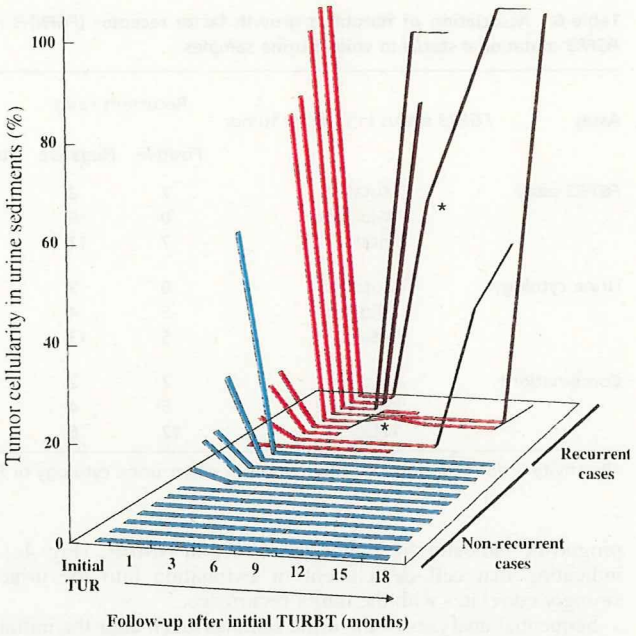


Fig. 5. The time-course analysis of tumor cellularity in the voided urine sediments in cases with mutated-fibroblast growth factor receptor (*FGFR*)-3. Tumor cellularities serially determined after initial transurethral resection of bladder tumor (TURBT) are plotted on 3-D line chart. All cases had *FGFR3* mutations in their tumor tissues. Red and blue lines indicate the data of recurrent ($n$ = 9) and non-recurrent ($n$ = 12) cases, respectively. Two asterisks indicate the events of positive results prior to the cystoscopical detection of recurrent tumors. In recurrent cases, the last point of serial determination indicates tumor cellularity in the preoperative urine sediments obtained before second TURBT.

Estimated from Poisson distribution, the probability of missing mutated FGFR3 molecules was 4.98% on sampling the aliquot containing *FGFR3* mutations at the concentration of 1% in 1 ng of the genomic DNA. The probabilities of missing mutated DNA molecules in the template increased up to 13.5% for two copies and 35.8% for a single copy, resulting in frequent false negatives. These assumptions suggested that 1% of tumor cellularity in 1 ng of the template DNA is actually the minimal detectable dose in the assay.

We developed a quantitative method to determine the proportion of *FGFR3* mutations in the sample as tumor cellularity and this approach disclosed the correlation between tumor cellularity and intravesical recurrence of NMIBC.

Assessing the risk for intravesical recurrence and progression after TURBT is another major concern in the clinical management of NMIBC. Many efforts have been reported to establish any molecular alterations in tumor tissues as prognostic markers.[2,20] Although some earlier studies have analyzed *FGFR3* mutation as a potential prognostic marker, the true prognostic value of *FGFR3* mutation is still controversial.[21–23] Quantitative analysis revealed that the tumor cellularity in the preoperative urine sediments strongly correlates with the tumor recurrence ($P$ = 0.008). Moreover, the ROC analysis of the preoperative urine sediments determined the optimal cut-off value of *FGFR3* mutations (11%) in the urine sediments that differentiates between the recurrent and non-recurrent tumors (Fig. 4). Using this cut-off value, the sensitivity, specificity, and diagnostic accuracy for detecting tumor recurrence were 77.8, 83.3, and 80.9%, respectively. This is the first report elucidating that the *FGFR3* mutational status in the urine sediments may serve as a



doi: 10.1111/j.1349-7006.2009.01334.x

Table 6. Association of fibroblast growth factor receptor (*FGFR*)-3 mutational status in primary tumors with cytological examination and/or *FGFR3* mutational status in voided urine samples

| Assay | *FGFR3* status in primary tumor | Recurrent cases | | Non-recurrent cases | | Assay performance | | | |
|---|---|---|---|---|---|---|---|---|---|
| | | Positive | Negative | Positive | Negative | Sensitivity (%) | Specificity (%) | Accuracy (%) | *P*-value |
| *FGFR3* assay | Mutated | 7 | 2 | 0 | 15 | 78 | 100 | 92 | 0.0001 |
| | Wild-type | 0 | 9 | 1 | 11 | 0 | 92 | 52 | 1.0000 |
| | Total | 7 | 11 | 1 | 26 | 39 | 96 | 73 | 0.0042 |
| Urine cytology | Mutated | 0 | 9 | 0 | 15 | 0 | 100 | 63 | NA |
| | Wild-type | 5 | 4 | 0 | 12 | 56 | 100 | 81 | 0.0062 |
| | Total | 5 | 13 | 0 | 27 | 28 | 100 | 71 | 0.007 |
| Combination† | Mutated | 7 | 2 | 0 | 15 | 78 | 100 | 92 | 0.0001 |
| | Wild-type | 5 | 4 | 1 | 11 | 56 | 92 | 76 | 0.0464 |
| | Total | 12 | 6 | 1 | 26 | 67 | 96 | 84 | <0.0001 |

†Positivity is defined by the positive result in either urine cytology or FGFR3 mutation detection assay. NA, not analyzed.

prognostic indicator for tumor recurrence in NMIBC (Fig. 4c), indicating that cell detachment or exfoliation into the urine strongly correlates with the tumor recurrence.

Sequential analyses of the urine samples taken after the initial TURBT revealed intravesical recurrence in almost 78% (7/9) of the recurrent cases showing *FGFR3* mutations in the primary tumors, while the cytological examination of the same sample showed no positive results (Table 6). In two cases, *FGFR3* mutations were detected prior to the cystoscopical detection, indicating that the urine *FGFR3* assay can diagnose intravesical recurrence reliably in the postoperative management of NMIBT cases harboring *FGFR3* mutations in primary tumors. As shown in Table 6, the sensitivity of *FGFR3* mutations and urine cytology in the follow-up samples were mutually exclusive, indicating that the combination of urine *FGFR3* assay and cytological examinations improved diagnostic sensitivity in detecting tumor relapse. van Rhijn *et al.* reported that the median sensitivity of the cytology for patients under surveillance was 48% and varied between histological grades, ranging from 17% for Grade 1, 34% for Grade 2, and 58% for Grade 3.[24] In the present study, the proportion of tumor grades was 13% (6/45), 78% (35/45), and 9% (4/45) for Grades 1, 2, and 3. Grade 1 and 2 tumors occupied more than 90% of the cohort and the sensitivities of urine cytology in the recurrent cases were 0% (0/9) and 56% (5/9) depending on the presence or absence of the *FGFR3* mutations.

In conclusion, our results indicate the potential usefulness of the urine *FGFR3* mutation assay as both a significant predictor of intravesical recurrence and a complementary urinary marker for monitoring patients undergoing TURBT in combination with urine cytology. Once *FGFR3* mutations are detected in the primary tumors, the patients should be indicated for monitoring *FGFR3* mutations in the urine sediments, particularly when the tumor cellularity in the preoperative urine sediments is above the cut-off level of 11%.

## Acknowledgements

This work was supported in part by a Grant-in-Aid for Cancer Research and for the 3rd Term Comprehensive 10-Year Strategy for Cancer Control from the Ministry of Health, Labor, and Welfare, Japan. Makito Miyake, MD is the awardee of a Research Resident Fellowship from the Foundation for Promotion of Cancer Research (Japan) for the 3rd Term Comprehensive 10-Year Strategy for Cancer Control (Tokyo, Japan).

## Disclosure Statement

None.

## References

1 Parkin DM, Bray F, Ferlay J, Pisani P. Global cancer statistics, 2002. *CA Cancer J Clin* 2005; **55**: 74–108.
2 Sugano K, Kakizoe T. Genetic alterations in bladder cancer and their clinical applications in molecular tumor staging. *Nat Clin Pract Urol* 2006; **3**: 642–52.
3 Wiener HG, Mian C, Haitel A, Pycha A, Schatzl G, Marberger M. Can urine diagnostic tests replace cystoscopy in the management of bladder cancer? *J Urol* 1998; **159**: 1876–80.
4 Sidransky D, Von Eschenbach A, Tsai YC *et al.* Identification of p53 gene mutations in bladder cancers and urine samples. *Science* 1991; **252**: 706–9.
5 Mao L, Schoenberg MP, Scicchitano M *et al.* Molecular detection of primary bladder cancer by microsatellite analysis. *Science* 1996; **271**: 659–62.
6 Sugano K, Tsutsumi M, Nakashima Y *et al.* Diagnosis of bladder cancer by analysis of the allelic loss of the p53 gene in urine samples using blunt-end single-strand conformation polymorphism. *Int J Cancer* 1997; **74**: 403–6.
7 Shigyo M, Sugano K, Fukayama N *et al.* Allelic loss on chromosome 9 in bladder cancer tissues and urine samples detected by blunt-end single-strand DNA conformation polymorphism. *Int J Cancer* 1998; **78**: 425–9.
8 van Rhijn BW, Lurkin I, Kirkels WJ, van der Kwast TH, Zwarthoff EC. Microsatellite analysis-DNA test in urine competes with cystoscopy in follow-up of superficial bladder carcinoma: a phase II trial. *Cancer* 2001; **92**: 768–75.
9 Shigyo M, Sugano K, Tobisu K, Tsukamoto T, Sekiya T, Kakizoe T. Molecular followup of newly diagnosed bladder cancer using urine samples. *J Urol* 2001; **166**: 1280–5.
10 Steiner G, Schoenberg MP, Linn JF, Mao L, Sidransky D. Detection of bladder cancer recurrence by microsatellite analysis of urine. *Nat Med* 1997; **3**: 621–4.
11 van Rhijn BW, Lurkin I, Chopin DK *et al.* Combined microsatellite and *FGFR3* mutation analysis enables a highly sensitive detection of urothelial cell carcinoma in voided urine. *Clin Cancer Res* 2003; **9**: 257–63.
12 Johnson DE, Williams LT. Structural and functional diversity in the FGF receptor multigene family. *Adv Cancer Res* 1993; **60**: 1–41.
13 Billerey C, Chopin D, Aubriot-Lorton MH *et al.* Frequent *FGFR3* mutations in papillary non-invasive bladder (pTa) tumors. *Am J Pathol* 2001; **158**: 1955–59.
14 Kimura T, Suzuki H, Ohashi T, Asano K, Kiyota H, Eto Y. The incidence of thanatophoric dysplasia mutations in *FGFR3* gene is higher in low-grade or superficial bladder carcinomas. *Cancer* 2001; **92**: 2555–61.
15 Rieger-Christ KM, Mourtzinos A, Lee PJ *et al.* Identification of Fibroblast Growth Factor Receptor 3 mutations in urine sediment DNA samples complements cytology in bladder tumor detection. *Cancer* 2003; **98**: 737–44.
16 van Oers JM, Lurkin I, van Exsel AJ *et al.* A simple and fast method for the simultaneous detection of nine Fibroblast Growth Factor Receptor 3 mutations in bladder cancer and voided urine. *Clin Cancer Res* 2005; **11**: 7743–8.

17 Miyake M, Sugano K, Kawashima K *et al.* Sensitive detection of *FGFR3* mutations in bladder cancer and urine sediments by peptide nucleic acid-mediated real-time PCR clamping. *Biochem Biophys Res Commun* 2007; **362**: 865–71.
18 Sobin LH, Wittekind C, eds. *TNM Classification of Malignant Tumors*, 6th edn. New York: John Wiley & Sons, 2002.
19 Mostofi FK, Sobin LH, Torloni H. *Histological Typing of Urinary Bladder Tumors: International Classification of Tumors, No. 10*. Geneva: World Health Organization, 1973: 21–31.
20 Knowles MA. Role of *FGFR3* in urothelial cell carcinoma: biomarker and potential therapeutic target. *World J Urol* 2007; **25**: 581–93.
21 van Rhijn BW, Lurkin I, Radvanyi F, Kirkels WJ, van der Kwast TH, Zwarthoff EC. The fibroblast growth factor receptor 3 (*FGFR3*) mutation is a strong indicator of superficial bladder cancer with low recurrence rate. *Cancer Res* 2001; **61**: 1265–8.
22 Hernández S, López-Knowles E, Lloreta J *et al.* Prospective study of *FGFR3* mutations as a prognostic factor in nonmuscle invasive urothelial bladder carcinomas. *J Clin Oncol* 2006; **24**: 3664–71.
23 Burger M, van der Aa MN, van Oers JM *et al.* Prediction of progression of non-muscle-invasive bladder cancer by WHO 1973 and 2004 grading and by *FGFR3* mutation status: a prospective study. *Eur Urol* 2007; **54**: 835–43.
24 van Rhijn BW, van der Poel HG, van der Kwast TH. Urine markers for bladder cancer surveillance: a systematic review. *Eur Urol* 2005; **47**: 736–48.



doi: 10.1111/j.1349-7006.2009.01334.x

Clinical Cancer Research

# Combined Functional Genome Survey of Therapeutic Targets for Hepatocellular Carcinoma

Reiko Satow[1], Miki Shitashige[1], Yae Kanai[2], Fumitaka Takeshita[3], Hidenori Ojima[2], Takafumi Jigami[1], Kazufumi Honda[1], Tomoo Kosuge[4], Takahiro Ochiya[3], Setsuo Hirohashi[1,2], and Tesshi Yamada[1]

## Abstract

**Purpose:** The outcome of patients with advanced hepatocellular carcinoma (HCC) has remained unsatisfactory. Patients with HCC suffer from chronic hepatitis or liver cirrhosis, and their reserve liver function is often limited.

**Experimental Design:** To develop new therapeutic agents that act specifically on HCC but interfere only minimally with residual liver function, we searched for genes that were upregulated in 20 cases of HCC [namely, discovery sets 1 ($n$ = 10) and 2 ($n$ = 10)] in comparison with corresponding nontumorous liver and a panel representing normal organs using high-density microarrays capable of detecting all exons in the human genome.

**Results:** Eleven transcripts whose expression was significantly increased in HCC were subjected to siRNA-based secondary screening of genes required for HCC cell proliferation as well as quantitative reverse transcription-PCR analysis [validation sets 1 ($n$ = 20) and 2 ($n$ = 44)] and immunohistochemistry ($n$ = 19). We finally extracted four genes, *AKR1B10*, *HCAP-G*, *RRM2*, and *TPX2*, as candidate therapeutic targets for HCC. siRNA-mediated knockdown of these candidate genes inhibited the proliferation of HCC cells and the growth of HCC xenografts transplanted into immunodeficient mice.

**Conclusions:** The four genes we identified were highly expressed in HCC, and HCC cells are highly dependent on these genes for proliferation. Although many important genes must have been overlooked, the selected genes were biologically relevant. The combination of genome-wide expression and functional screening described here is a rapid and comprehensive approach that could be applied in the identification of therapeutic targets in any type of human malignancy. *Clin Cancer Res; 16(9); 2518–28. ©2010 AACR.*

Liver cancer is the fifth most common human cancer worldwide and the third most common cause of cancer mortality. Hepatocellular carcinoma (HCC) is the most common histologic subtype of liver cancer and is highly endemic in Southeast Asia and sub-Saharan Africa (1). HCC develops mainly in liver affected by chronic hepatitis or cirrhosis caused by persistent infection with hepatitis B or C virus; however, the precise molecular mechanisms that drive the transition from the background liver conditions to cancer are largely unknown. Liver resection, ethanol injection, radiofrequency ablation, and chemoembolization have been used successfully for the local management of HCC; however, no single cytotoxic chemotherapeutic agent has been proven effective for the systemic treatment of HCC; thus, the outcome for patients with locally advanced, multicentric, and/or metastatic HCC who are not eligible for these local treatments has remained unsatisfactory.

An increasing number of therapeutic agents targeting molecular components essential for cancer cell growth have begun to be incorporated into oncological practice: Imatinib, which blocks the Bcr-Abl fusion kinase of chronic myeloid leukemia (CML), is currently the first-line therapy for CML (2). The epidermal growth factor receptor inhibitors gefitinib and erlotinib have been used in the treatment of advanced non–small cell lung cancer (3). Recently, it was shown in a phase III study that sorafenib (BAY 43-9006), a multikinase inhibitor, significantly improved the overall survival of patients with advanced HCC (4, 5), and, consequently, sorafenib has since been approved for the treatment of patients with unresectable HCC by the American Food and Drug Administration. However, most patients enrolled in those studies retained relatively well-compensated

**Authors' Affiliations:** [1]Chemotherapy Division, [2]Pathology Division, and [3]Section for Studies on Metastasis, National Cancer Center Research Institute; and [4]Hepatobiliary and Pancreatic Surgery Division, National Cancer Center Hospital, Tokyo, Japan

**Note:** Supplementary data for this article are available at Clinical Cancer Research Online (http://clincancerres.aacrjournals.org/).

Microarray data from this study have been submitted to the Gene Expression Omnibus database (accession no. GSE12941).

**Corresponding Author:** Tesshi Yamada, Chemotherapy Division, National Cancer Center Research Institute, 5-1-1 Tsukiji, Chuo-ku, Tokyo 104-0045, Japan. Phone: 81-3-3542-2511; Fax: 81-3-3547-6045; E-mail: tyamada@ncc.go.jp.

**doi:** 10.1158/1078-0432.CCR-09-2214

## Translational Relevance

Liver cancer is the fifth most common human cancer worldwide and the third most common cause of cancer mortality. Recently, a multikinase inhibitor, sorafenib, has been approved as a systemic chemotherapeutic drug for advanced hepatocellular carcinoma (HCC); however, further improvement seems to be necessary. To identify an "Achilles heel" of HCC cells and develop new therapeutic agents that act specifically on HCC but interfere only minimally with residual liver function, we performed an unbiased survey of the whole genome. We finally identified four genes as candidates. siRNA-mediated knockdown of these candidate genes inhibited the proliferation of HCC cells and the growth of HCC xenografts transplanted into immunodeficient mice, confirming their feasibility as therapy targets.

liver function. In reality, the reserve liver function of HCC patients is often limited due to underlying liver conditions. Therefore, the safety and tolerability of sorafenib remain to be determined in HCC patients with compromised liver function. Therapeutic targeting molecules other than protein kinases have also been developed against various tumors of other organs (6–8). To identify a molecule essential for HCC cell growth and develop new therapeutic agents that would act specifically on HCC and only minimally interfere with residual liver function, a survey of the whole genome would be necessary.

In this study, we adopted a combined functional approach. We first searched for genes that were upregulated in HCC in comparison with the background nontumorous liver tissue. This was followed by siRNA-based screening of genes required for HCC cell proliferation. Recently, whole-genome RNA interference (RNAi)–based functional screening has been reported to successfully identify genes that sensitize lung cancer cells to a chemotherapeutic drug and genes required for proliferation and survival of several cancer cell lines; however, in those studies, the expressional specificity of the identified targets was not taken into consideration (9–12). Here, we report the identification of possible therapeutic target molecules of HCC through a combination of genome-wide expression and functional screening.

## Materials and Methods

***Patients and microarray analysis.*** Samples of HCC and surrounding nontumorous liver tissue were collected from 84 patients who underwent liver resection for HCC at the National Cancer Center Hospital (Tokyo, Japan) with informed consent. The clinical and histologic data for these patients are summarized in Supplementary Table S1. Total RNA of normal human organs was obtained from a commercial source (FirstChoice Human Total RNA Survey Panel, Ambion).

One microgram of total RNA was converted to end-labeled cRNA using a Whole Transcript Sense Target Labeling kit (Affymetrix). The fluorescent cRNA probes were hybridized to Human Exon 1.0 ST arrays (Affymetrix), as instructed by the supplier. Data analysis was carried out using the ArrayAssist software package (version 5.5.1, Stratagene). A GC content-based background correction followed by quantile normalization was done with an exonRMA algorithm available in the package. Multiple exonic expression data were also summarized into a single value using the same algorithm, as instructed by the supplier (http://www.stratagene.com/manuals/ArrayAssist.pdf).

The protocol of this study was reviewed and approved by the ethics committee of the National Cancer Center (Tokyo, Japan).

***Cell lines.*** Three human cell lines derived from HCC were used in this study. KIM-1 was kindly provided by Dr. Masamichi Kojiro (Kurume University, Kurume, Japan). Hep3B was obtained from the Cell Resource Center for Biomedical Research, Tohoku University (Sendai, Japan). HLE was obtained from the Health Science Research Resources Bank (Osaka, Japan). KIM-1 and Hep3B were maintained in RPMI 1640 (Invitrogen) supplemented with 10% fetal bovine serum. HLE was maintained in Dulbecco's modified Eagle's medium (Invitrogen) supplemented with 10% fetal bovine serum.

***siRNA-based functional screening.*** The day before siRNA transfection, cells were seeded at $5 \times 10^3$ per well in 96-well plates to obtain 50% to 60% confluency. They were then transfected with siRNA using Lipofectamine 2000 (Invitrogen) at a concentration of 10, 20, or 50 nmol/L in KIM1, Hep3B, or HLE cells, respectively. Three days later, the relative proportion of living cells was assessed using a Premix WST-1 Cell Proliferation Assay System (Takara Bio) in accordance with the manufacturer's instructions. The siRNA was synthesized by Ambion, and the identification (ID) numbers of siRNAs used in this study are listed in Supplementary Table S4. Silencer Negative Control #1 siRNA (Ambion) was used as a nontargeting control. siRNA targeting *TOP2A* was described previously (13).

***Real-time PCR.*** First-strand cDNA was synthesized from 1 μg of total RNA using SuperScript reverse transcriptase (Invitrogen). Real-time PCR was done as described previously (14). Primers and probes sets were obtained from Applied Biosystems, and their Assay IDs are provided in Supplementary Table S5. The amplification reaction was done according to the manufacturer's instructions (95°C for 10 minutes followed by 40 cycles of 95°C for 15 seconds, 50°C for 2 minutes, and 60°C for 1 minute).

***Immunohistochemistry and immunoblot analysis.*** Anti-AKR1B10 (clone 1A6) and anti–HCAP-G (clone 4B1) monoclonal antibodies were purchased from Abnova. Anti-RRM2 antibody (E-16) was purchased from Santa

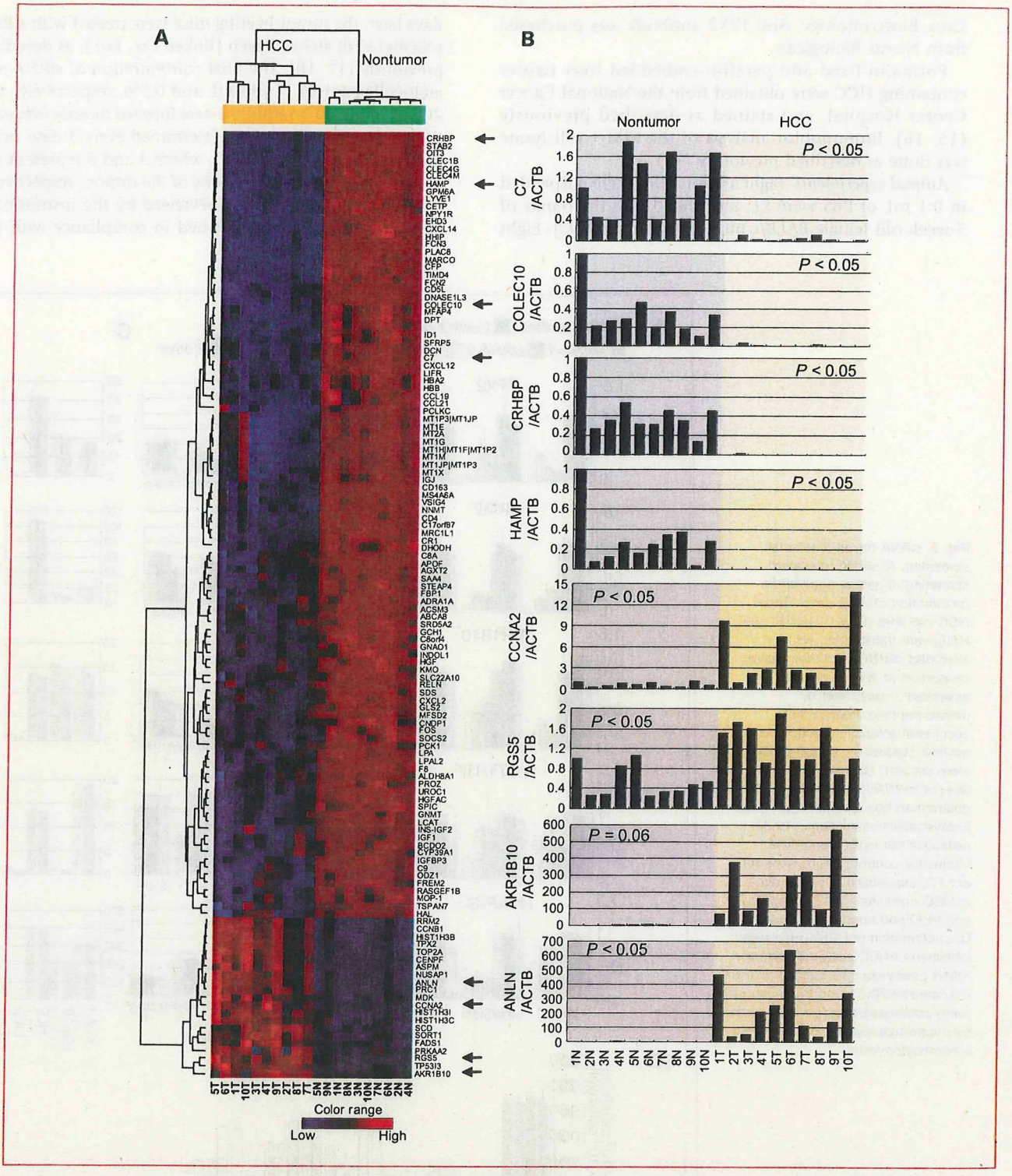


**Fig. 1.** Genes differentially expressed between HCC and nontumorous liver. A, hierarchical clustering of 124 genes whose expression differed significantly ($P < 0.001$ and >3-fold change) between HCC and adjacent nontumorous liver. Transcriptional signal intensity is shown as a heat map. Red indicates higher signals, whereas blue indicates lower signals. Arrows indicate eight genes selected for validation by real-time PCR (B). B, validation of the microarray data by real-time RT-PCR. The expression levels of eight representative genes whose expression differed significantly between adjacent nontumorous liver (left) and HCC (right) were validated by real-time RT-PCR (shown in arbitrary units). Significant correlation between array (discovery set 1) and real-time RT-PCR data was confirmed by calculating correlation coefficient values in eight randomly selected genes (indicated by arrows in A): *C7*, 0.96; *COLEC10*, 0.97; *CRHBP*, 0.98; *HAMP*, 0.98; *CCNA2*, 0.82; *RGS5*, 0.80; *AKR1B10*, 0.98; *ANLA*, 0.92. The significance of differential expression between HCC and adjacent nontumorous liver tissue was assessed using a permutation paired *t* test, and Bonferroni-corrected *P* values are provided.

Cruz Biotechnology. Anti-TPX2 antibody was purchased from Novus Biologicals.

Formalin-fixed and paraffin-embedded liver tissues containing HCC were obtained from the National Cancer Center Hospital, and stained as described previously (15, 16). Immunoblot analysis of the KIM-1 cell lysate was done as described previously (15).

***Animal experiments.*** Eight million KIM-1 cells suspended in 0.1 mL of PBS were s.c. inoculated into the flanks of 5-week-old female BALB/c nu/nu nude mice (SLC). Eight days later, the tumor-bearing mice were treated with siRNA together with atelocollagen (Koken Co., Ltd.), as described previously (17, 18). The final concentration of siRNA and atelocollagen was 11 μmol/L and 0.5%, respectively, and 200 μL of the siRNA solution were injected directly into each tumor. Tumor volume was determined every 3 days using the formula $V = 1/2\ (A \times B^2)$, where $A$ and $B$ represent the largest and smallest dimensions of the tumor, respectively.

Animal experiments were reviewed by the institutional ethics committee and performed in compliance with the

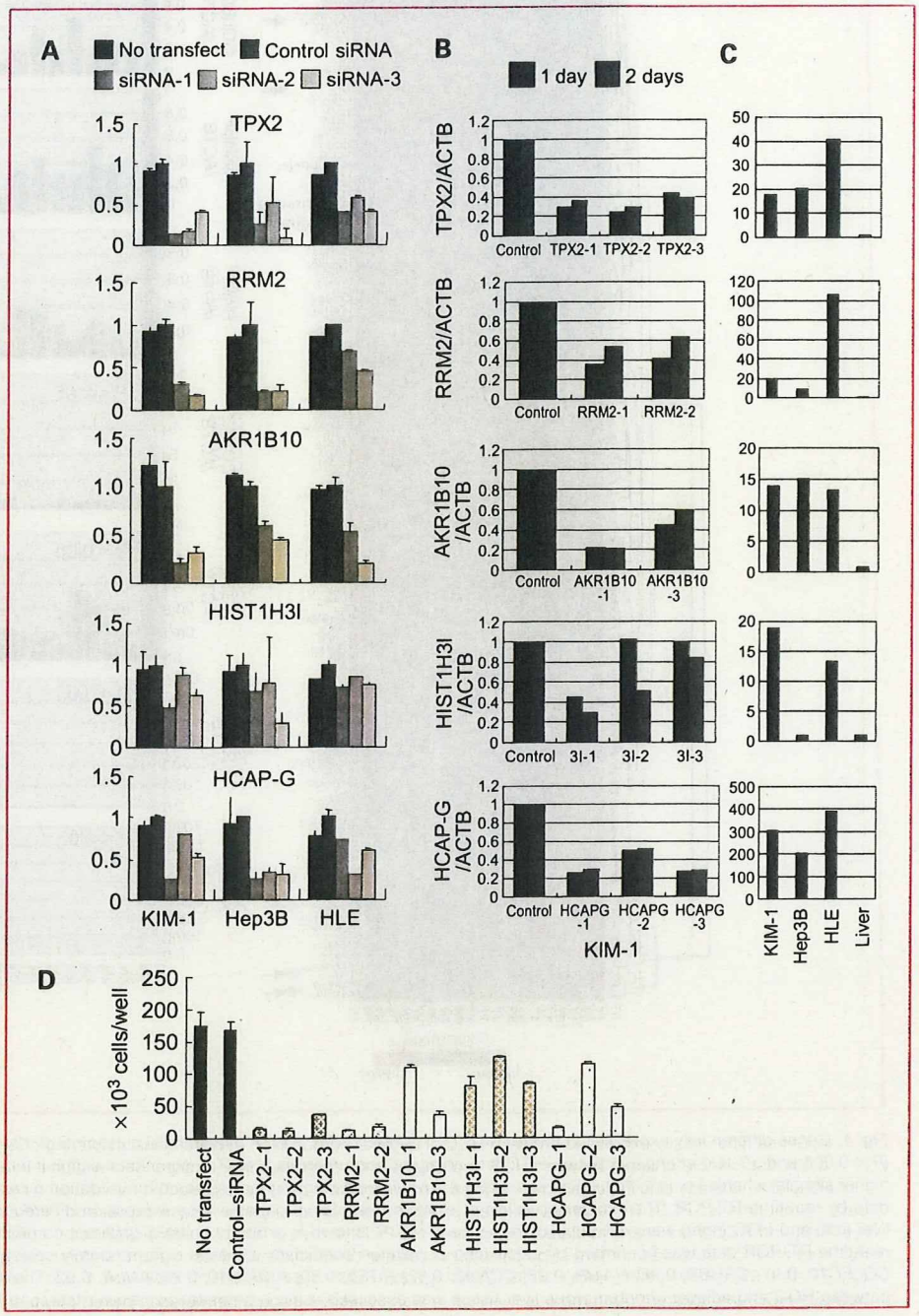


**Fig. 2.** siRNA-based functional screening. A, siRNA-mediated screening of genes required for proliferation of HCC cells. Three HCC cell lines (KIM-1, Hep3B, and HLE) were transfected with the indicated siRNAs, and the relative proportion of living cells was assessed 3 days later by measuring the mitochondrial succinate-tetrazolium reductase activity. Values for control siRNA were set at 1. B, reduction of the level of mRNA for each gene was determined by real-time PCR 1 and 2 days after transfection of KIM-1 cells with the indicated siRNAs. Values for control siRNA were set at 1. C, expression of each gene in HCC cell lines (KIM-1, Hep3B, and HLE) and normal liver tissue. D, confirmation of siRNA-mediated inhibition of HCC cell proliferation. KIM-1 cells were transfected with the indicated siRNAs, and the number of living cells was counted 3 days later by trypan blue dye exclusion using a hemocytometer.

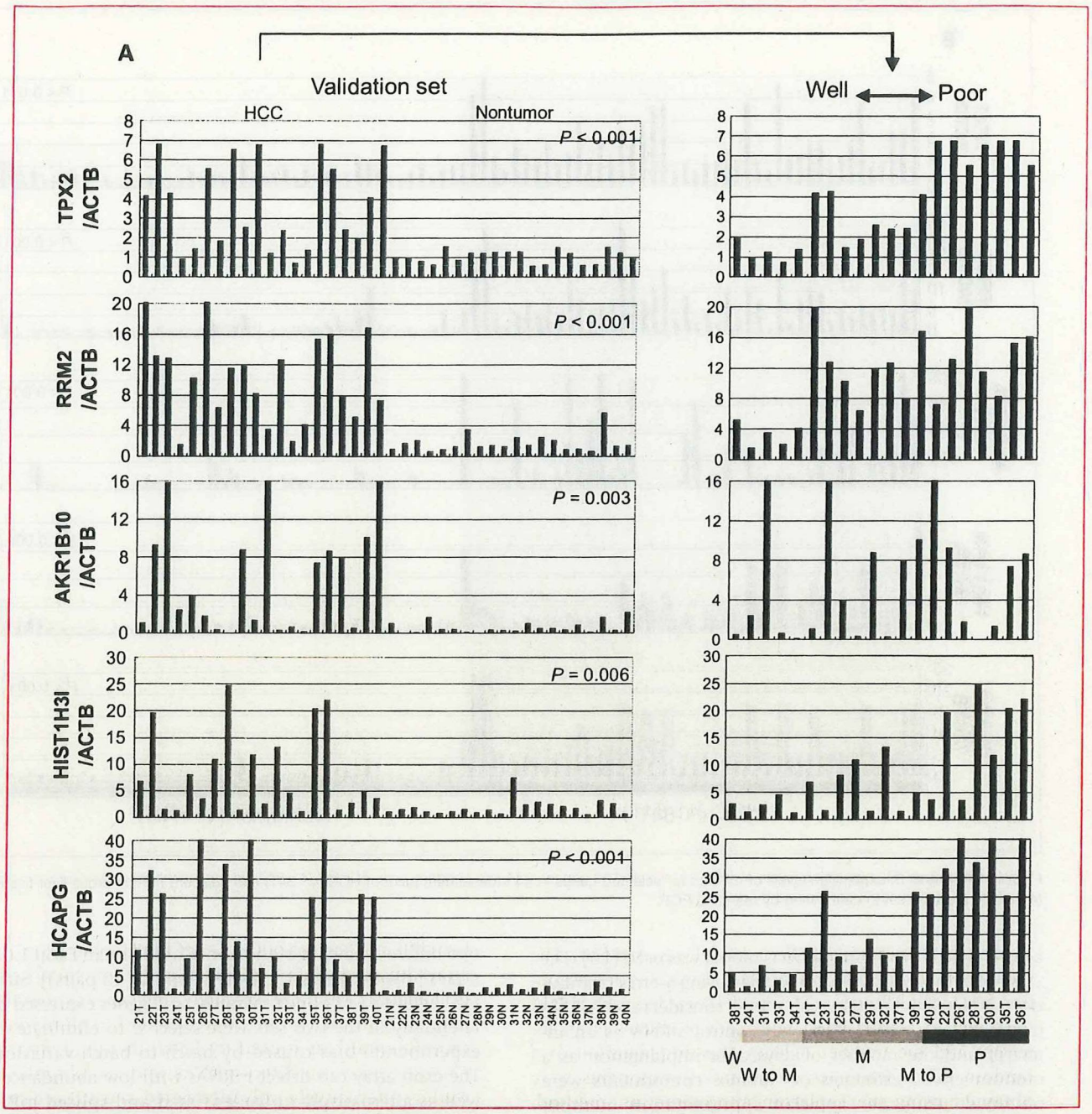


**Fig. 3.** Validation of differential expression. A, mRNA expression levels of selected genes in 20 independent pairs of HCC (21-40T) and adjacent nontumorous liver tissue (21-40N; validation set 1) determined by real-time PCR (left). The expression levels in HCC were realigned according to histologic differentiation (right). W, well differentiated; W to M, well to moderately differentiated; M, moderately differentiated; M to P, moderately to poorly differentiated, P, poorly differentiated.

guidelines for Laboratory Animal Research of the National Cancer Center Research Institute (Tokyo, Japan).

***Statistical analysis.*** To extract differentially expressed genes from the array data, a paired *t* test with no correction was done (19) with asymptotic distribution to determine the *P* value. Correlations between array data and real-time PCR measurements were assessed using the Pearson correlation coefficient. The significance of differential gene expression between HCC and adjacent nontumorous liver tissue was assessed using the permutation paired *t* test followed by Bonferroni correction.

The weights and volumes of tumors are given as means (+SE). To evaluate the chronological effect of siRNAs on the growth of xenografts in comparison with control siRNA,